AFWL-TR-
69-101

SPALL STUDIES ON 6061-T6 ALUMINUM

Charles Jajosky, Jr.
Capt USAF

Mark A. Fordman
Lt USAF

TECHNICAL REPORT NO. AFWL-TR-69-101

September 1969

AIR FORCE WEAPONS LABORATORY
Air Force Systems Command
Kirtland Air Force Base
New Mexico

92

AFWL-TR-69-101

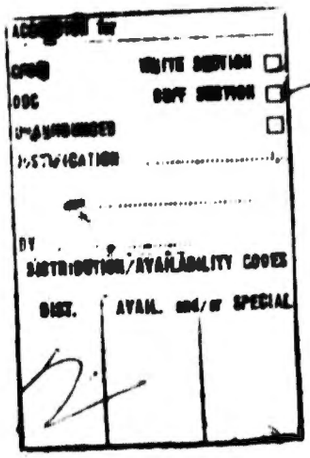

AIR FORCE WEAPONS LABORATORY
Air Force Systems Command
Kirtland Air Force Base
New Mexico

When U. S. Government drawings, specifications, or other data are used for any purpose other than a definitely related Government procurement operation, the Government thereby incurs no responsibility nor any obligation whatsoever, and the fact that the Government may have formulated, furnished, or in any way supplied the said drawings, specifications, or other data, is not to be regarded by implication or otherwise, as in any manner licensing the holder or any other person or corporation, or conveying any rights or permission to manufacture, use, or sell any patented invention that may in any way be related thereto.

This report is made available for study with the understanding that proprietary interests in and relating thereto will not be impaired. In case of apparent conflict or any other questions between the Government's rights and those of others, notify the Judge Advocate, Air Force Systems Command, Andrews Air Force Base, Washington, D. C. 20331.

DO NOT RETURN THIS COPY. RETAIN OR DESTROY.

BLANK PAGE

SPALL STUDIES ON 6061-T6 ALUMINUM

Charles Jajosky, Jr.
Captain USAF

Mark A. Ferdman
Lieutenant USAF

TECHNICAL REPORT NO. AFWL-TR-69-101

FOREWORD

This research was performed under Program Element 6.16.46.01.H, Project 5710, Subtask 15.025, and was funded by the Defense Atomic Aupport Agency (DASA).

Inclusive dates of research were January 1968 to March 1969. The report was submitted 24 July 1969 by the Air Force Weapons Laboratory Project Officer, Lt Mark A. Ferdman (WLRP).

Information in this report is embargoed under the U.S. Export Control Act of 1949, administered by the Department of Commerce. This report may be released by departments or agencies of the U.S. Government to departments or agencies of foreign governments with which the United States has defense treaty commitments, subject to approval of AFWL (WLRP).

This technical report has been reviewed and is approved.

Mark A. Ferdman

MARK A. FERDMAN
Lieutenant, USAF
Project Officer

Harry F Rizzo

HARRY F. RIZZO
Lt Colonel, USAF
Chief, Physics Branch

Thomas L Franklin Col.

CLAUDE K. STAMBAUGH
Colonel, USAF
Chief, Research Division

ABSTRACT

(Distribution Limitation Statement No. 2)

Flat specimens of 32 mil 6061-T6 aluminum were dynamically shock loaded by high velocity Mylar flyer plates. A 16 kilojoule capacitor discharge system and exploding foil assemblies were used to accelerate 3, 5, 7.5, and 10 mil Mylar flyers at spall threshold velocities between 0.5 and 2 mm/μsec. The environment between flyer and target was both normal atmospheric air and vacuum. The observed apparent spall threshold and spall depths in air differed significantly from those obtained in vacuum. The air layer has the effect of reducing the amplitude of the induced stress pulse and spreading the shock front and/or its pulse duration. The spall threshold data were analyzed and an attempt was made to apply available predictive models. The data best fit the Tuler, et al., model, with a stress exponent of 1.8. This condition very closely approximates a pure-energy criterion for spallation.

This page intentionally left blank.

CONTENTS

ILLUSTRATIONS

ILLUSTRATIONS (Cont'd)

TABLES

ABBREVIATIONS AND SYMBOLS

Tmax	maximum value of tension at spall plane (spall stress)
σ_e	elastic stress, kb
λ	exponent in failure criterion, dimensionless
K	constant in failure criterion, $(kb)^{\lambda}$ microsec.
σ_o	level-off stress in failure criterion, kb
K1	value of K in cgs units, $\left(\frac{dynes}{cm^2}\right)^{\lambda}$ seconds
$\bar{S}_1$, $\bar{S}_2$, $\bar{S}_3$	distances to 1st, middle, and final damage plane, mils
d	standard deviation, dimensionless
M	best fit slope relating spall depth to flyer thickness, $^{mil}/_{mil}$
C	correlation coefficient, dimensionless
H_p	projectile thickness, mils
H_t	target thickness, mils
ρ, ρo	density after and before impart, $^{gms}/_{cm^3}$
V, Vo	specific volume after and before impart, $^{cm^3}/_{gms}$
ε_o	volume strain, dimensionless
$\dot{\varepsilon}$	volume strain rate, sec^{-1}
E	Young's modulus, $^{dynes}/_{cm^2}$
Up	particle velocity, $^{cm}/_{microsec.}$
Co	sound speed, $^{cm}/_{microsec.}$
P_H	pressure along Hugoniot, $^{dynes}/_{cm^2}$
θ	coef. in relation $Us = \theta U_p + Co$, dimensionless
Us	shock velocity, $^{cm}/_{microsec.}$
C, D, S	coefs. in equation $P_H = C_\mu + D_\mu^2 + S_\mu^3$, $^{dynes}/_{cm^2}$
Ce	elastic wave velocity, $^{cm}/_{microsec.}$

ABBREVIATIONS AND SYMBOLS (Cont'd)

μ	compressibility = $\frac{\rho - \rho u}{\rho o}$, dimensionless
X	position, cm
t	time, seconds
A	parameter = $K^{1/\lambda}$, k,λ as defined above, $(kb)(\mu sec)^{1/\lambda}$
ss	sum of squares of deviations, dimensionless
Z_f, Z_t	impedence of flyer, tgt. materials, $^{gm}/cm^2$ μsec
S_A, S_R	constants in equations relating V_c^A, V_c^R to H_p, $\left(^{mm}/microsec.\right)\left(mils\right)^{1/\lambda}$
Vo	level off velocity, ^{cm}/microsec.
U_s^f	sound speed in flyer, ^{cm}/microsec.
U_s^t	sound speed in target, ^{cm}/microsec.
ψ	$S_A - S_R$, $\left(^{mm}/microsec.\right)\left(mils\right)^{1/\lambda}$

SECTION I

INTRODUCTION

The use of thin flyer impact experiments to evalute the dynamic strength of materials has long been instrumental in providing information on the susceptibility of missile systems to nuclear weapon effects. Use of the technique requires a thorough understanding of the experimental procedures and dynamic material properties. The development of reentry vehicle and missile systems requires long lead times. Mylar shots can be performed in vacuum environments quite rapidly. Unfortunately, the latter class of experiments has been difficult to understand, because of the cushioning effect of the air between the flyer and the target material. This study is an investigation of the effect of this air layer. The results and analysis of a recent set of experimental data produced with and without an air layer are presented. An additional objective of this study is to examine the generality of empirical models for the prediction of the dynamic failure response of 6061-T6 aluminum, chosen as the target material. Mylar was chosen as the flyer material since it has a lower shock impedance than the target material, aluminum. With the use of a flyer having an impedance lower than the target, a single rectangular shock pulse is induced in the target. Also, Mylar can be obtained in thin sheets. Flyer thicknesses of 3, 5, 7.5, and 10 mil were used.

In addition, this report provides the reader with an overall idea of the basic theory, equipment, measurement techniques, and analytical tools currently available. It presents the results and recommends suggestions for further research.

The section on theoretical discussion includes a treatment on mathematically fitting an empirical equation to the experimental data and deriving values for the parameters in that equation. However, the reader should not lose sight of the fact that the primary purpose of this study is not to describe

the spall behavior of aluminum but rather to see whether or not pulse power experiments conducted in an air environment can give meaningful and useful results.

The shots performed in an air environment were based on work from a thesis by Captain J. R. Baca (Ref. 1).

SECTION II

APPROACH

The high-velocity impact by a thin plate produces shock pulse with a very fast rise in flat samples of 6061-T6 aluminum. In this work, the aluminum targets were impacted with high-velocity, thin Mylar flyer plates. When the Mylar impacts the aluminum surface, a compressive shock wave is generated at the interface by the decrease of flyer particle velocity and the rapid increase in target particle velocity. The magnitude of the pressure generated by such an impact is proportional to the flyer velocity and the shock impedances of both the flyer and target materials. The stress wave thus generated propagates into both flyer and target, away from the impact surfaces. When this shock wave reaches the rear or free-surface of the flyer, a relief wave forms. This relief wave then propagates back toward the flyer-target interface. When it arrives at the interface, the flyer rebounds away from the target because the interface cannot support the tensile stress. A rarefaction wave is formed at the new free surface and propagates toward the rear surface of the target. The result is the formation of a complete rectangular stress pulse whose duration is approximately twice the transit time of the Mylar flyer. When the front of this shock pulse arrives at the rear free surface of the target, it is reflected and forms a rarefaction wave moving toward the target impact surface. As this wave intersects with the relief wave in the compressive shock, a tensile pulse forms If this tension is large enough in both amplitude and duration, failure occurs. This process of compressive and tensile wave formation and propagation is simplified in Figure 1.

For this effort, failure is described as the creation of voids in a solid body by the action of a stress. It can be divided into a sequence of

a. Crack nucleation

b. Crack growth

In ductile failure there is considerable plastic flow before and during crack growth. In brittle failure, the mean crack velocity is rapid because very little flow occurs before separation. Spallation is fracture by short duration tensile

pulses. Incipient spall is considered, in this report, to be the condition in which voids are just visible at 50x magnification. 6061-T6 has a face-centered cubic lattice and does not exhibit brittle-type failure except in cases of grain boundary embrittlement. It has been reported (Ref. 2) that in 6061-T6 Al the voids form at inclusion sites, and often show distortion indicative of plastic flow within the matrix. The fracture appears to be mostly ductile, even though the strain rates encountered in plate-slap experiments are very high.

The failure of 6061-T6 aluminum, using this procedure, was investigated in both air and vacuum environments to see whether or not there is any significant advantage in evacuating the experimental chamber.

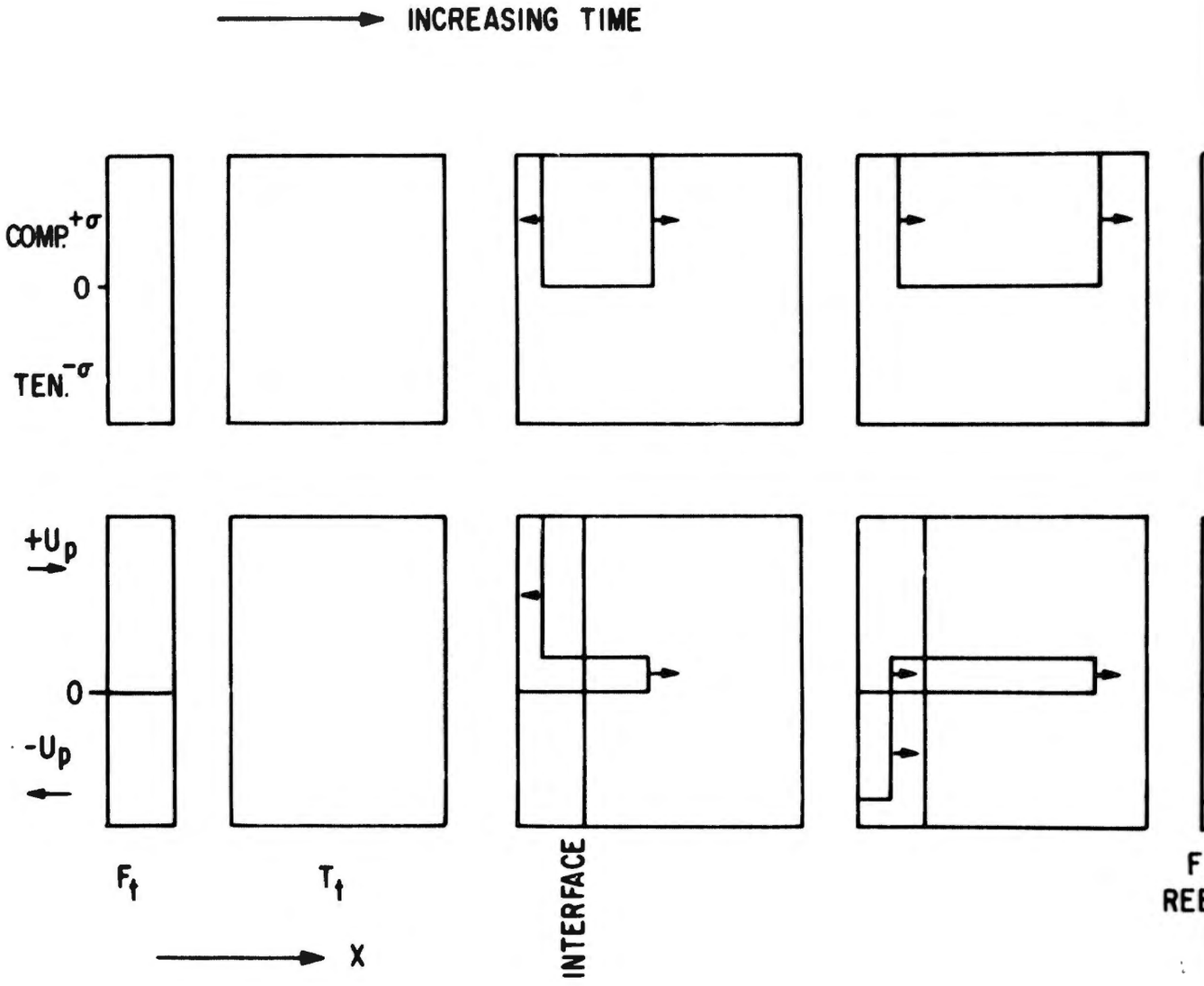
INCREASING TIME
COMP. $+\sigma$
0
TEN. $-\sigma$
$+U_p$
0
$-U_p$
F_f
T_f
INTERFACE
X

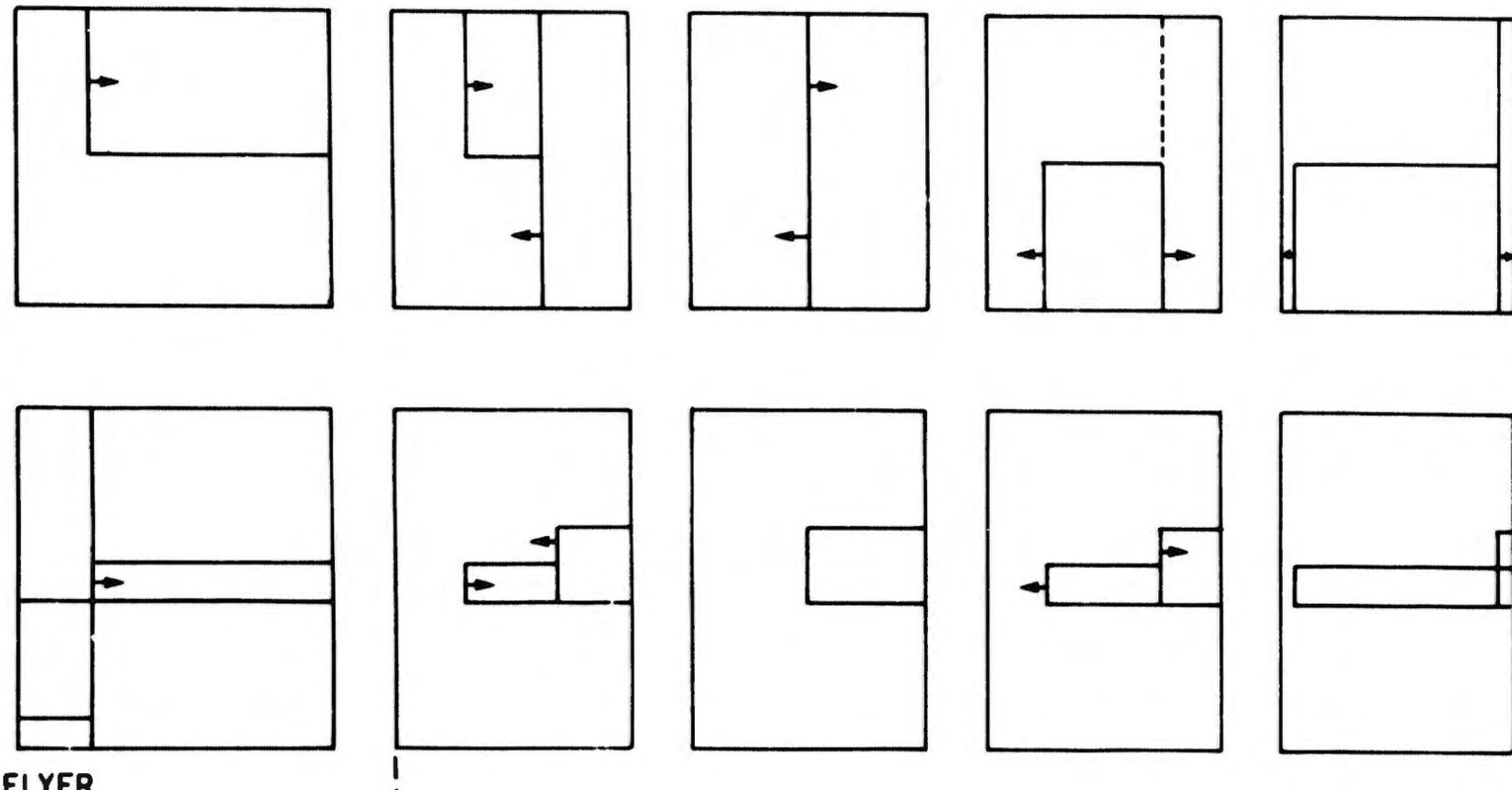

Figure 1. Str

B

NCREMENT BETWEEN THESE FRAMES CORRESPONDS TO THE Δt FOR SPALL

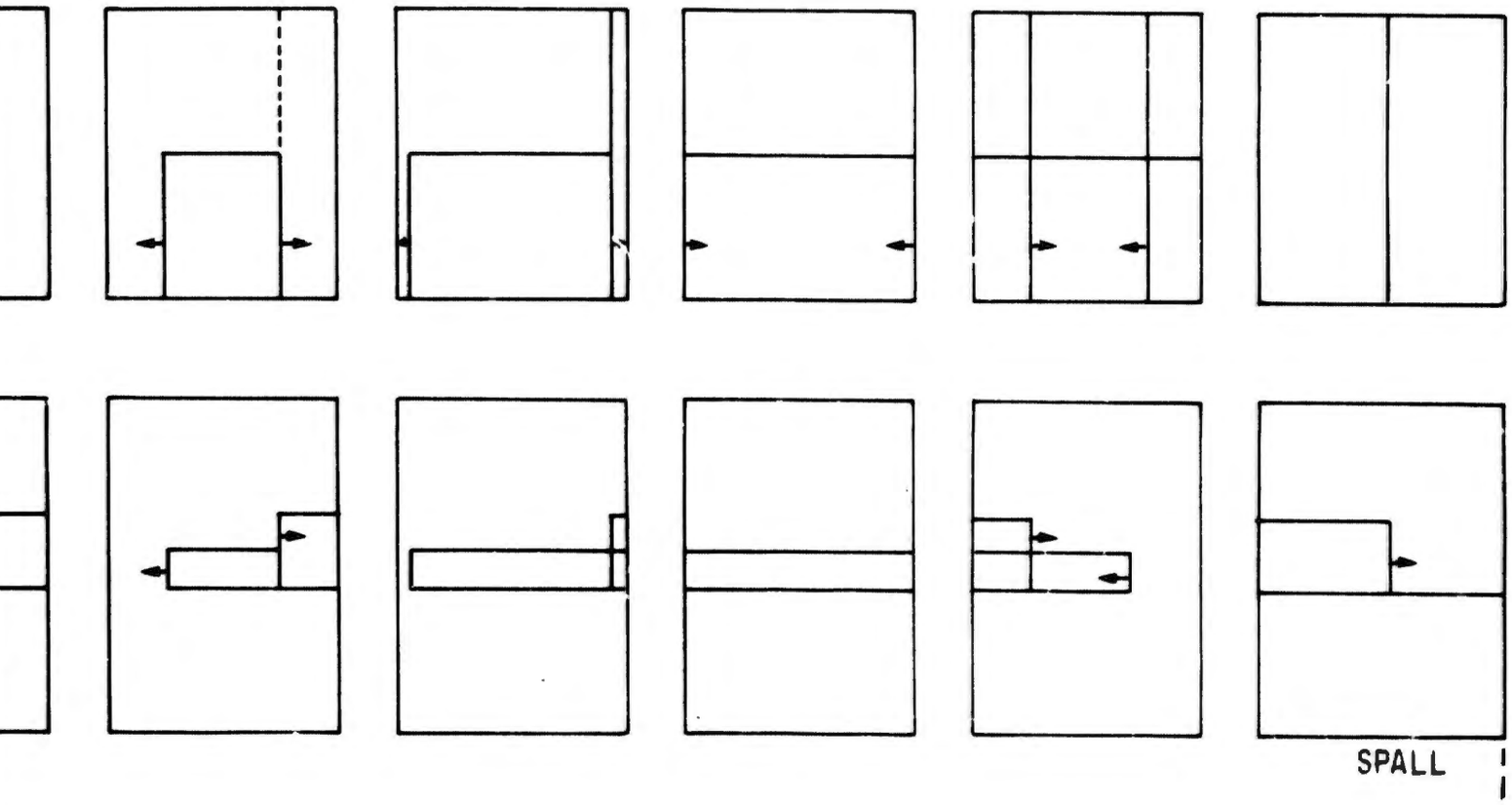

FOLLOWING DIAGRAMS (AFTER REBOUND)

ARROWS SHOW RELATIVE DIRECTION OF STRESS WAVE AND PARTICLE MOTION

Figure 1. Stress-wave Interactions

This page intentionally left blank.

SECTION III

THEORETICAL DISCUSSION

1. INTRODUCTION

This section examines the available experimental data from the standpoint of shock wave physics. It is quite apparent that not enough data exist to warrant a thoroughly rigorous analysis. However, the authors felt that it would be meaningful to attempt to apply the basic shock wave equations to the data in the best way possible. The results can be used as guidelines for future experimental work, and to see how well future results correlate with the predicted model.

At present, the AFWL facility has generated the following data for impacting Mylar on 6061-T6 Al:

a. Critical velocity for spall versus flyer thickness of 3.0, 5.0, 7.5, and 10.0 mil flyers on 32 mil targets in air.

b. Critical velocity for spall versus flyer thickness of 5.0, 7.5, and 10.0 mil flyers on 32 mil targets in a vacuum

c. Measurements of average spall depth as a function of flyer thickness for both the air and vacuum shots.

2. STRAIN RATE

The typical stress-time history at the flyer-target interface for a typical flyer plate experiment is shown in Figure 2. This pressure-time history was generated by the P-PUFF material response code (Ref. 3). For an explanation of the symbols used in this and all remaining sections, the reader is referred to the list of abbreviations and symbols appearing at the beginning of the report.

To estimate the induced strain rate, the magnitude of the peak compression and pulse width are determined from a typical profile. Figure 3 shows the Hugoniot data in (P_H - u) space for 6061-T6 (Ref. 4). The 5 mil vacuum shot required a critical velocity for spall of approximately 1 mm/μsec. According to the resulting profile at the first zone (P-PUFF uses a finite-difference scheme) in the target, a compression pulse of 40 kb magnitude was produced

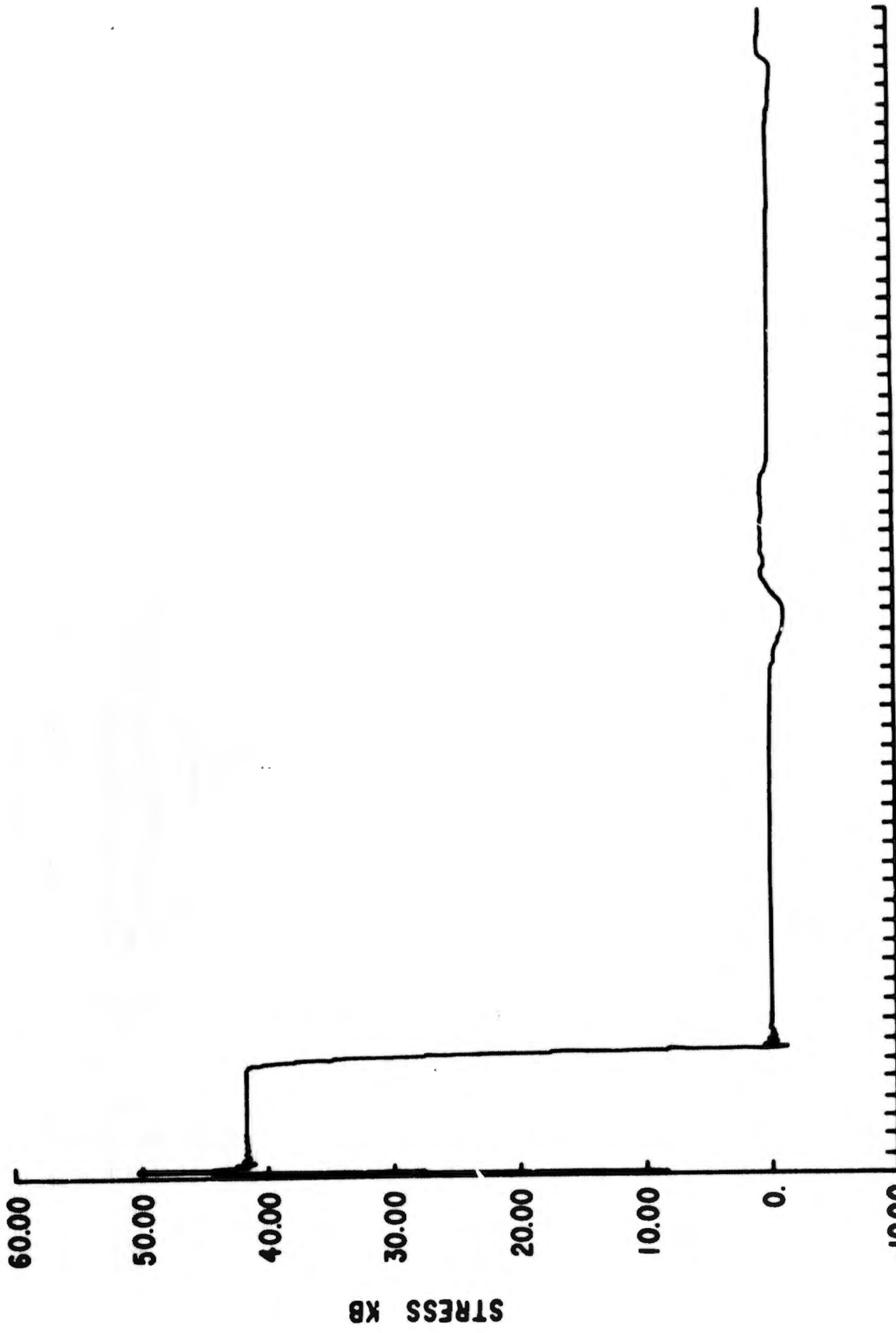

Figure 2. Initial Compressive Pulse

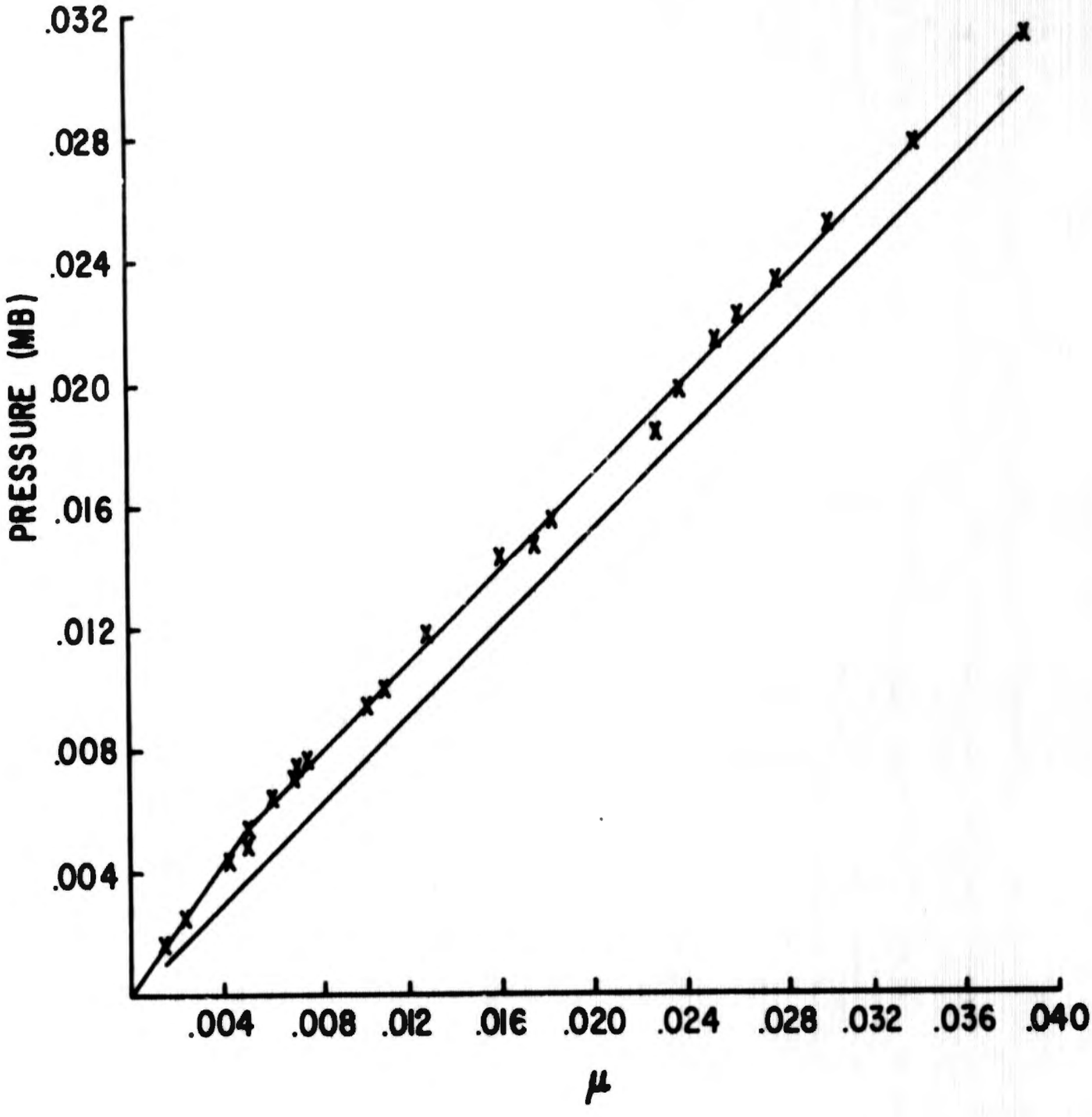

Figure 3. 6061-T-6 Hugoniot

with a corresponding time at maximum stress of approximately 0.1 μsec ($\approx 10^{-7}$ second). By extrapolating the curve in Figure 3 it is seen that for this pressure the corresponding compression (μ) is approximately 0.05, where μ is defined by the expression

$$\mu = \frac{\rho - \rho o}{\rho o} = \frac{Vo - V}{Vo}$$

and ρo, Vo = density, specific volume prior to compression

ρ, V = density, specific volume following compression.

The volume strain is the same as μ so that the volume strain rate, designated as $\dot{\epsilon}$, can be approximated as follows:

$$\dot{\epsilon} \approx \frac{\mu}{(\text{Time to peak comp.})} \approx \frac{0.050}{10^{-7}} \approx 10^5 - 10^6/\text{sec.}$$

The typical strain rates thus encountered are extremely high, and only at very long pulse widths does the response of the material approach static values.

3. EQUATION OF STATE

The rate of crack propagation in a material is often considerably less than the rate of stress waves through the material, since crack growth is proportional to the acoustic velocity, and shock wave velocity (Us) is related to acoustic velocity (Co) by an expression of the form

$$Us = \theta\, Up + Co$$

where Up = induced particle velocity,

θ = material constant.

Thus it is possible for cracks to form in a material without any extensive growth during the typically short times in shock experiments. In the limiting case of an infinite number of cracks, then no growth at all would be required for spall.

The situation of minimum growth corresponds to incipient spall, where the voids are of characteristically small size. The exact definition of what corresponds to incipient spall is completely arbitrary. In this report, incipient spall refers to that extent of failure just visible at 50x magnification.

Spall is failure caused by the reflection of compression waves as tensile pulses, which in turn create particle velocities in a direction opposite that of the tensile pulse propagation. If a material is impacted completely within the elastic range, the corresponding elastic wave velocity is given by

$$Ce = \left(\frac{E}{\rho o}\right)^{1/2}$$

where E = Young's elastic modulus

ρo = initial density

Ce = elastic wave velocity

The following is derived by application of the Hugoniot equation for momentum conservation:

$$\sigma_e = \text{elastic stress} = \rho o \; Ce \; Up$$

$$E = \frac{d\sigma_e}{d\varepsilon} = C_e^{\,2} \rho o \text{ where } \varepsilon = \text{volume strain}$$

$$Up = \frac{\sigma_e}{\rho o Ce} = \frac{\rho o \int_o^{\varepsilon} C_e^{\,2} \; \varepsilon}{\rho o \; Ce} = \int_o^{\varepsilon} Ce \; d\varepsilon$$

For most spall shots, the strains induced are well above the Hugoniot elastic limit (Ref. 5), and a two wave structure is produced. The strain rates typically encountered are of the order of 10^5 to 10^6/sec (see preceding section) and the yield point of the material increases significantly over the static value. Figure 4 shows a typical Us-Up plot, and illustrates the fact that for high pressures the linear relation

$$Us = \theta \; Up + Co$$

is obeyed with the extrapolated value, Co, corresponding approximately to the bulk sound speed. In the elastic region, the linear relation is no longer obeyed. The experimentally determined Hugoniot elastic limit for 6061-T6 is about 5.4 kb (Ref. 4). The experiments described in this report produced impact stresses of

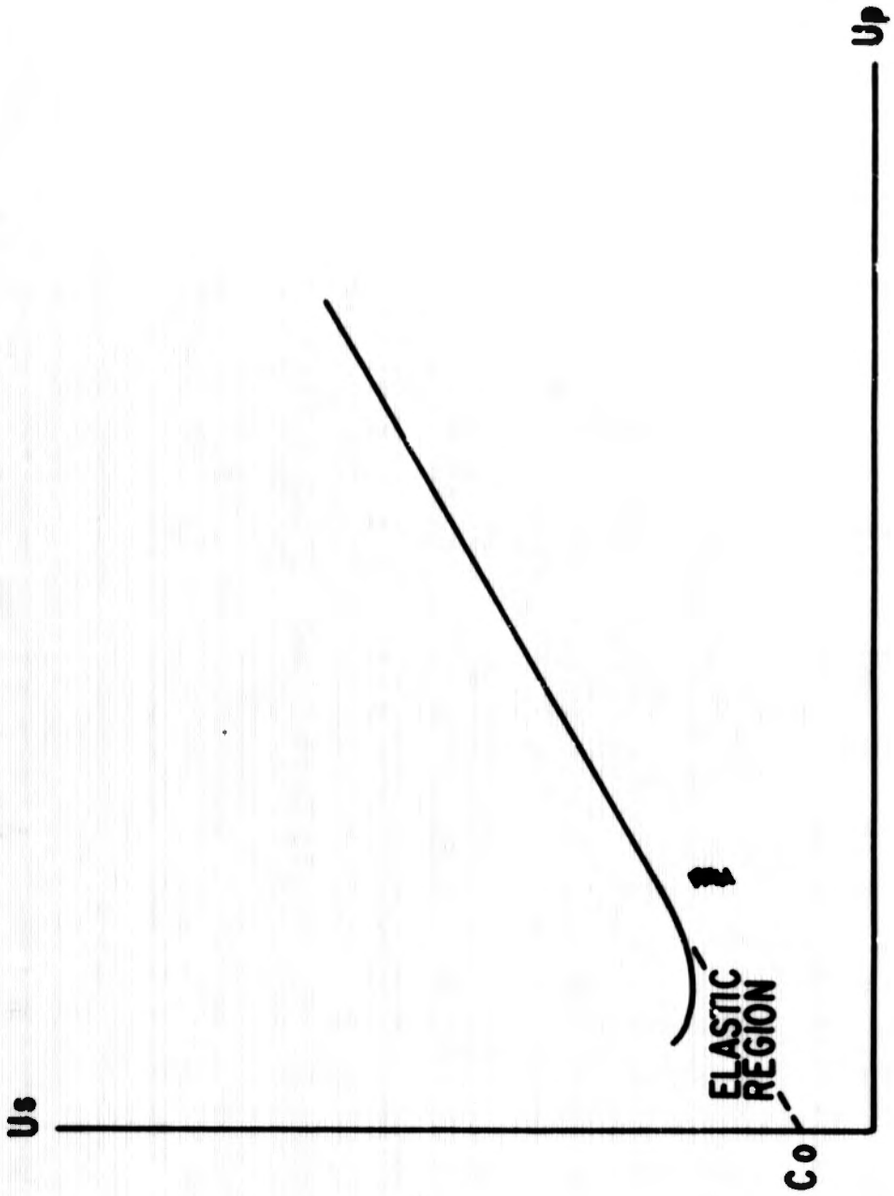

Figure 4. Typical Us-Up Plot

20 kb and higher, significantly in the plastic regime. A condition for Hugoniot shots is that uniaxial strain is assumed, so that a comparison with normal tensile data is only possible by utilizing the equations for converting uniaxial stress data to uniaxial strain. Thus, for the experiments discussed in this report, the material undergoes plastic deformation, and since the equation

$$Us = \theta\ Up + Co$$

is obeyed for plastic deformation, some alteration of the material properties does have a chance to occur before crack formation.

The equation above is particularly well suited for analysis of Hugoniot equation-of-state data. An alternate method is to attempt a least-squares fit for P_H (Hugoniot pressure) as a function of μ (compression) of the form

$$P_H = C\mu + D\mu^2 + S\mu^3 \text{ (Ref. 3)}$$

where C, D, S are material constants. The Hugoniot equation for momentum conservation for a plastic wave can be written as

$$P_H = \rho o\ Up\ (Co + \theta Up)$$

We can use these two expressions to equate P_H as a function of μ using the values of Co and θ:

$$P_H = \frac{\rho o\ Co^2\ \mu\ (\mu + 1)}{[1 + \mu\ (1 - \theta)]^2}$$

Thus, there are two basic ways to characterize the Hugoniot data:

a. Measurements of Co and θ to relate P_H and μ.

b. Measurement of P_H and μ directly, and finding the C, D, S values from a least-squares fit.

If Co and θ are known, then one can plot P_H versus μ and do a least-squares fit to find C, D, S.

For analysis of spall conditions suitable equation-of-state information must be put into P-PUFF for both the flyer and target materials. The iuput parameters to P-PUFF relating to material properties are as follows (Ref. 3):

RHO: Density $\left(gm/cm^3\right)$

EQSTC, EQSTD, EQSTS: C, D, S coefs. above $\left(dynes/cm^2\right)$

EQSTG*: Gruniesen coefficient (dimensionless)

EQSTE: Sublimation energy

EQSTH: $(\gamma - 1)$ for small $\left(\frac{\rho}{\rho_0} - 1\right)$ where $\gamma = \frac{C_P}{C_v}$

YO: Initial yield strength $\left(dynes/cm^2\right)$

YADD: Slope of yield strength curve $dynes/cm^2$

YMU: Compression (μ) at elastic limit (dimensionless)

The values for equation-of-state data for 6061-T6 aluminum are known fairly well. The figures shown in Table I are based on data generated by Sandia Corporation (Ref. 4). The values for Mylar are not nearly so well documented. One source of uncertainty lies in the fact that Mylar is obtainable only in thin sheets typically on the order of 0.014 inch. To make Hugoniot measurements, an accurate determination of shock transit time is required. With thin samples the error introduced into these measurements makes an accurate Hugoniot determination difficult. Another source of undertainty in determination of a Hugoniot point is the lack of knowledge of the thermal contribution to induced pressure.

The Mylar equation of state given in Table I is based on values from Boeing Document D2-90099. It was chosen since a preliminary investigation showed that it yielded results most nearly duplicating the response of 6061-T6 aluminum as predicted by impacting 6061-T6 aluminum on a target of the same material.

4. FAILURE CRITERION

In a shock wave experiment the stress at a point in the material is a function of both position and time. Since a case of one-dimensional strain is assumed, only the X-coordinate is applicable, and the stress, σ, can be expressed as

$$\sigma = \sigma(x,t)$$

σ = stress

---

* Defined thermodynamically as $\frac{1}{V}\left(\frac{\partial P}{\partial E}\right)_V$

TABLE I

EQUATION-OF-STATE PARAMETERS

	RHO	EQSTC	EQSTD	EQSTS	EQSTG	EQSTE	YO	YMU	AMU
Mylar									
(file)	1.39	0.06728×10^{12}	0.14549×10^{12}	0.23627×10^{12}	1.00	4.4×10^{10}	0	0	0
6061-T6 Al									
Sandia (Ref. 3)	2.70	0.73398×10^{12}	1.85973×10^{12}	-26.98235×10^{12}	2.03	1.1768×10^{11}	2.69948×10^{9}	4.90526×10^{-3}	2.75162×10^{11}

The value of EQSTH is given as 0.25 in all cases. It should be emphasized that considerable data exist for other Mylar equations of state, and the values above correspond to just one set which has been employed at the Weapons Laboratory. These parameters are given only to orient the reader who may be familiar with the P-PUFF hydrocode.

x = coordinate position

t = time

The time factor is of particular importance in ductile failure where crack growth of relatively slow. The conditions will be such that tension is produced over a specific time interval.

F. R. Tuler and B. H. Butcher (Ref. 5) suggest a spall criterion of the form

$$(T_{max} - \sigma_o)^{\lambda} \Delta t = K$$

where

T_{max} = maximum spall stress

Δt = pulse duration measure at 1/2 T_{max}

λ, σ_o, K are dynamic material properties

Two general theories exist for determining failure:

a. Time-dependent

b. Time-independent

One form, a stress gradient approach, leads to a relationship of the form (Ref. 6)

$$T_{max} = A + B \left(\frac{\partial \sigma}{\partial x}\right)^{1/2}$$

where A, B are, again, dynamic material properties. As pointed out in an article by researchers at McDonnell-Douglas Astronautics (Ref. 7), such stress-gradient theories are independent of previous history at any given material location, and thus do not fully take into account the effects of variations in pulse shape. The mechanical plate slap experiments described in this report produce essentially rectangular pulses, although an examination of the stress-time profile generated by the P-PUFF computer code indicates a significant variation in pulse-width from peak to zero stress. It is shown in the same article (Ref. 7) that by utilizing the very general form of the failure criterion suggested by Tuler and Butcher, the stress gradient equation corresponds to a pure impulse criterion at short pulse widths ($\lambda = 1$). This criterion is a phenomenological one for predicting incipient spall.

In this report no assumption is made about the value of λ a priori, and the value is used which best fits the experimental data. Thus no attempt is made to correlate the data on the basis of pure impulse ($\sigma\Delta t$).

In analyzing the spall data, one technique is to input the measured critical velocities for spall $\left(V_c^R\right)$ for the vacuum shots into P-PUFF and thus obtain stress-time profiles for each flyer thickness at the zone corresponding, as closely as possible, to the measured spall depth, $\bar{S}_2^R$ (for description of $\bar{S}_2^R$, see Section VI-1 on spall depth measurements). From the calculations of stress and pulse-width the dynamic response of the material under the specified conditions can be determined.

In attempting to analyze the spall data the following assumptions will be made:

a. The value of Tmax corresponds to the critical stress for spall.

b. The appropriate pulse width is that measured at 1/2 Tmax.

In terms of these quantities the failure criterion can be written as

$$(\text{Tmax} - \sigma o)^{\lambda}\Delta t = K$$

A typical plot of Tmax versus Δt for a ductile-type response appears as in Figure 5. The three identified regions are characteristic of most ductile materials. The region of "unpredictable behavior" corresponds to very high stresses at very short pulse widths. It is not at all clear that a material will continue to spall under increasingly higher stresses, approaching infinity, at extremely short pulse-widths. Since present experimental capabilities do not allow production of pulse widths less than about 10 nanoseconds, this region has not really been investigated thoroughly. Secondly, there is undoubtedly some stress level at which the atomic bonds split in an equicohesive manner, causing the curve to level off at a peak stress. In this report the curve will be graphically displayed only down to the shortest pulse width attained.

The "knee region" is the portion of maximum interest. The spall stress is still changing quite rapidly with pulse duration so that a very slight variation in pulse width results in a significant change in spall stress. The closer one gets to the level-off region, the less dramatic this effect becomes.

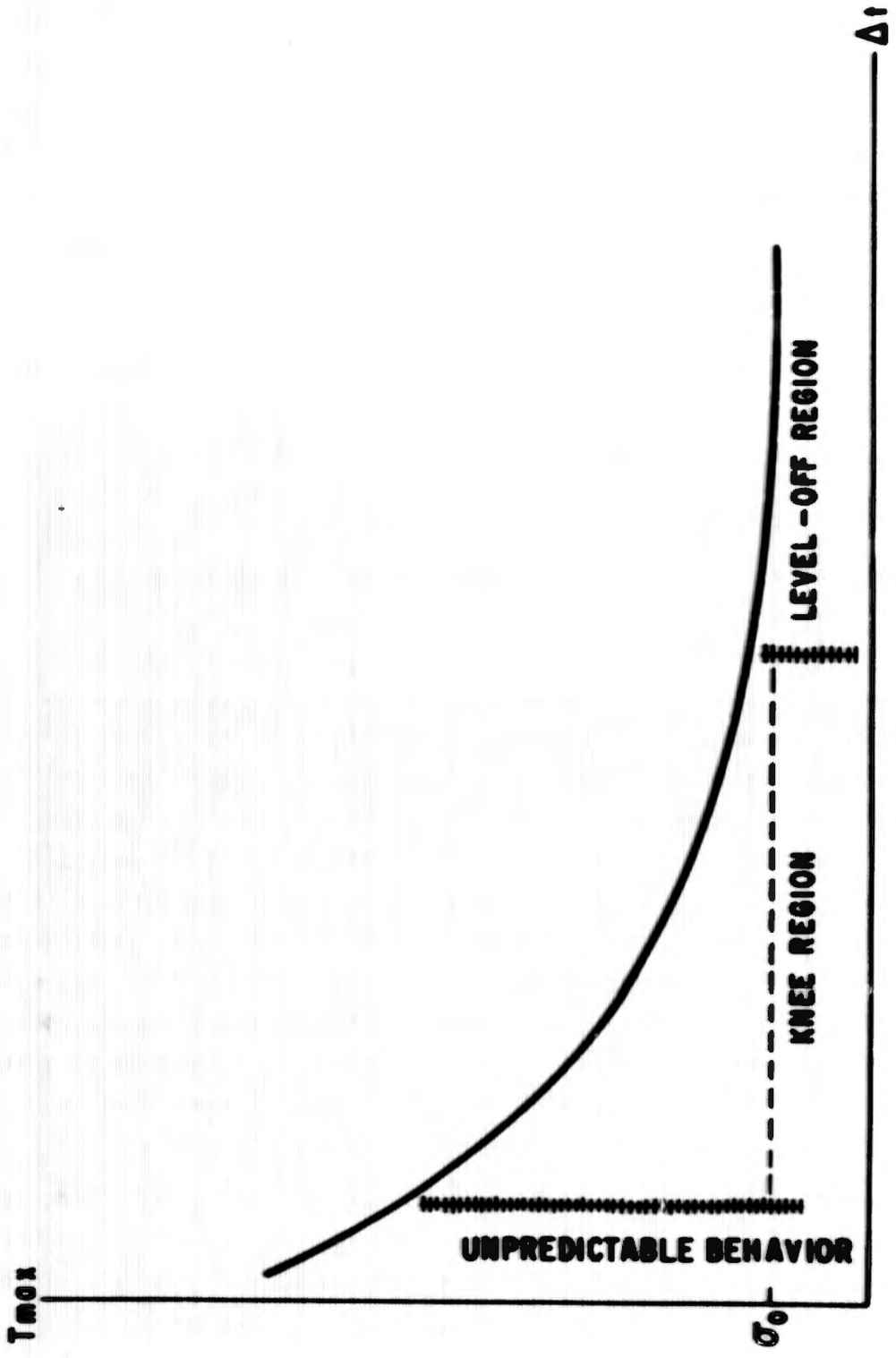

Figure 5. Typical σ versus Δt Response Curve

The "level-off" region is that segment for which the spall stress becomes very close to the value of σ_o. This factor is hard to determine without dynamic tests at very long pulse durations.

To determine a value of λ and K from the data, a least-squares analysis was performed. The original equation can be rewritten in the following form:

$$T_{max} = \sigma_o + K^{1/\lambda} \Delta t^{-1/\lambda}$$

or

$$T_{max} = \sigma_o + A \Delta t^{-1/\lambda}$$

where

$$A = K^{1/\lambda}$$

The values of Tmax and Δt have been determined experimentally for the three flyer thicknesses, 5, 7.5, and 10 mil, in a vacuum by obtaining stress-time profiles, using the P-PUFF material response code at the measured midplane of the spall region $\left(\bar{S}_2^R\right)$. For a given value of λ the best fit value of A is given by the expression

$$A = \left[\sum_j T_{max_j} \Delta t_j^{-1/\lambda} - \sigma_o \sum_j \Delta t_j^{-1/\lambda} \right] / \sum_j \Delta t_j^{-2/\lambda}$$

and the sum of the squares of the deviations, SS, is given by

$$SS = \sum_j \left[T_{max_j} - \left(\sigma_o + A \Delta t_j^{-1/\lambda} \right)^2 \right]$$

where the subscript j refers to a specific flyer thickness. Figure 6 shows a plot of SS versus λ for the experimental vacuum data. The minimum value of SS is obtained when $\lambda = 1.80$. The value of K is calculated by $K = A^{\lambda}$. The analysis for obtaining SS as a function of λ can be done using the computer-derived values of Tmax and Δt only for the vacuum data, since the problem of impact with an air cushion cannot be handled with a one-dimensional code such as P-PUFF 66.

All of the experimental data in this series of experiments suggest a value of λ from 1.80 to 2.0. The total area under a typical stress-strain curve is given approximately by

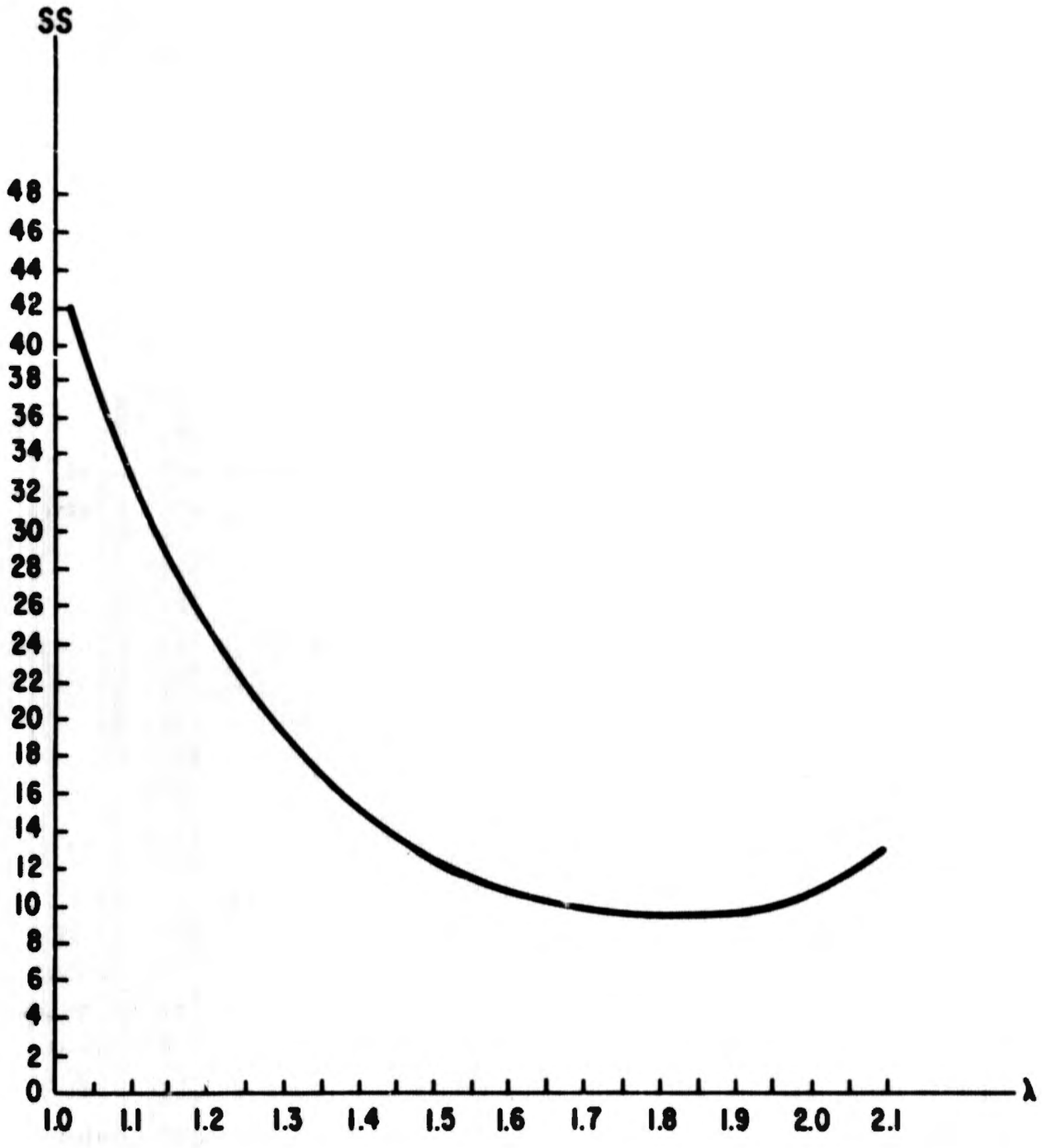

Figure 6. SS versus λ-Stress Data

$$1/2\ \varepsilon\ T_{max} \qquad \text{(linear } \sigma - \varepsilon \text{ approx.)}$$

and is proportional to the total energy expended in straining a material to the tension Tmax. Since one-dimensional strain is assumed, the substitution

$$\varepsilon = U_p \Delta t$$

should be approximately true, and if the conservation of momentum equation is applied, the result is

$$T_{max} = U_s\ U_p\ \rho_o$$

$$1/2\ \varepsilon\ T_{max} = \frac{1/2 T^2_{max}\ \Delta t}{U_s \rho_o} = \text{constant}$$

The important aspect of this equation is the product, $T^2_{max}\ \Delta t$, indicating that a criterion based on a critical energy for failure ought to have a value of $\lambda = 2.0$, as opposed to a value of 1.0 based on impulse.

If the general failure criterion is assumed to be

$$\left(T_{max} - \sigma_o\right)^{\lambda} \Delta t = K$$

then critical velocity data can be analyzed on the same basis. Linear theory predicts that the critical velocity for spall $\left(V_c^R\right)$ can be related to the spall stress, Tmax, by the relation

$$T_{max} = \frac{Z_P\ Z_T}{Z_P + Z_T}\ V_c^R$$

where Z_P = impedance of flyer material and Z_T = impedance of target material. The representative pulse width should be very nearly equal to

$$\Delta t = \frac{2\ H_P}{U_S^P}$$

where U_s^F = shock speed in the flyer material at the induced stress-level. The failure criterion is based on the assumption that as the pulse width gets larger the stress for spall approaches some limiting value;

$$\lim_{\Delta t \to \infty} Tmax = \sigma_o$$

The same argument applies to the critical velocity for spall;

$$\lim_{\Delta t \to \infty} V_C^R = Vo$$

where Vo would be given as $Vo = \frac{Z_F + Z_T}{Z_F \quad Z_T} \sigma_o$

In considering some comparisons between shots in air and in vacuum it also seems reasonable to assert that

$$\lim_{\Delta t \to \infty} V_C^R = \lim_{\Delta t \to \infty} V_C^A = Vo$$

which, in effect, says that for thicker flyers, hence, thicker pulses, the effect of the air layer should decrease, and the shots in air should behave as in a vacuum.

Rewriting the failure criterion in terms of V_C^R and H_p gives

$$Tmax = \frac{Z_F \quad Z_T}{Z_F + Z_T} V_C^R - \left[\frac{\left(Z_F \quad Z_T\right)}{\left(Z_F + Z_T\right)}\right] V_o + K^{1/\lambda}\left(\frac{2H_p}{U_S^F}\right)^{-1/\lambda}$$

or

$$V_C^R = V_o + \frac{\left[K^{1/\lambda}\left(\frac{2}{U_S^F}\right)^{-1/\lambda}\left(Z_F + Z_T\right)\right]}{Z_F \quad Z_T} H_p^{-1/\lambda}$$

$$V_C^R = Vo + S_R H_p^{-1/\lambda}$$

where

$$S_R = \frac{\left[K^{1/\lambda}\left(\frac{2}{U_S^F}\right)^{-1/\lambda}\left(Z_F + Z_T\right)\right]}{Z_F Z_T}$$

It is assumed that the general relation applies to the air shots, except with a different value for the coefficient;

$$V_C^A = V_o + S_A H_p^{-1/\lambda}$$

These equations are of the same form as

$$Tmax = \sigma_o + AH_p^{-1/\lambda}$$

and a best-fit value of λ can be obtained the same way as before.

In this case, however, the analysis can be done on both the air and vacuum data since the directly measurable quantities V_C^A, V_C^R, and H_p are available from experiment. Also, it should be mentioned that the velocity expressions are strictly true only if the flyer and target Hugoniots show no curvature for the pressures encountered. This is not completely true, and thus the value of λ is not going to be exactly the value obtained from stress measurements. It is, however, a good way to get an estimate from direct experimental quantities. Again, the data yields values of λ closer to 2.0 than 1.0.

The condition can also be imposed that the limit of $\left(V_C^A - V_C^R\right)$ is zero as H_p approaches infinity, and a least-squares analysis performed (by stepping λ and calculating SS, as before) on the quantity

$$\psi = V_C^A - V_C^R = \left(S_A - S_R\right) H_p^{-1/\lambda}$$

which, based on the present data, gives a value of λ almost exactly equal to 2. This avoids the problem of not knowing a value of V_o beforehand (see next section).

5. EVALUATION OF σ_o and V_o

The calculated best-fit value of A depends upon the value of σ_o. The same holds true when computing S_A and S_R, as one has to know an approximate value of Vo.

Before techniques for evaluating σ_o and Vo are described it should be noted that the values of λ determined by least-squares fitting of velocity and stress data were done with σ_o and Vo equal to zero. This was done for two reasons:

a. Too little experimental data exist for a reasonable determination of σ_o and Vo, by means of extrapolation.

b. The value of λ determined by the present method does not depend, in a major way, on the input value of σ_o (or Vo). Table II shows the variation in λ using the vacuum stress data between σ_o = 0.0 and σ_o = 6.0 kb. In this case λ was evaluated using pulse widths measured at one-half of the spall stress, which is the standard in this report. It is seen that when the input value of σ_o is varied from zero to 6 kb, there is approximately a 15 percent charge in the best-fit calculated value of λ.

TABLE II

VARIATION OF λ WITH σ_o

1. σ_o = 0.0 kb λ = 1.9

   σ_o = 6.0 kb λ = 1.6

   % change = 15%

If sufficient experimental data exist at long pulse widths, then a reasonable estimate of σ_o and Vo could be made directly from direct Tmax versus Δt or V_C^R (V_C) versus H_p curves.

From Figure 7, it is seen that, ideally, an extrapolation of the function to the line corresponding to $H_p \rightarrow \infty$ would yield a value of Vo. The same is true for extrapolating Figure 8 to the Y-axis $\left(\text{where } H_p^{-1/\lambda} \rightarrow 0\right)$. Curves based on actual data will be presented later.

The amount of data available, however, is not adequate to obtain a valid extrapolation. The conclusion is that Vo is probably small (Vo < .1mm/μsec). The least-squares values of Vo determined for each independent critical velocity data set (cf. Section II on Experimental Results) bear this out to some extent.

6. PURE IMPULSE VERSUS ENERGY COMPARISON

By calculating the appropriate products it is possible to show that the existing data support a criterion of $\lambda = 2.0$ as opposed to a value of $\lambda = 1.0$.

Table III gives the results of these calculations. The stress-pulse-width products are given only for the vacuum shots, since the values of Tmax and Δt, based on P-PUFF results, are known directly only for these shots. It is clear that, in all cases, the product using $\lambda = 1.0$ has a greater standard deviation, which is consistent with the fact that the least-squares values of λ are all closer to 2.0.

7. APPROXIMATE ANALYSIS

The object in this section is to see how accurately one can approximate spall locations, stress amplitudes, and durations by simple calculations. To perform such an approximate analysis, certain assumptions are necessary:

a. Hugoniot data for flyer and target materials are available; or, as a minimum, flyer Hugoniot data and a bulk sound speed and normal density of the target are available.

b. The induced stress pulse is a simple, rectangular, single-wave structure which experiences insignificant degradation or attenuation prior to target spallation.

c. A single shock wave velocity value can be used for each stress state and for all depths of the material.

The first approximation that can be performed is that of stress duration, Δt. It is assumed that the initial rectangular stress pulse remains unchanged in shape as it propagates and then reflects from the target rear free surface. Thus, the Δt, which corresponds to the time that the spall depth experiences tension, is approximated as follows:

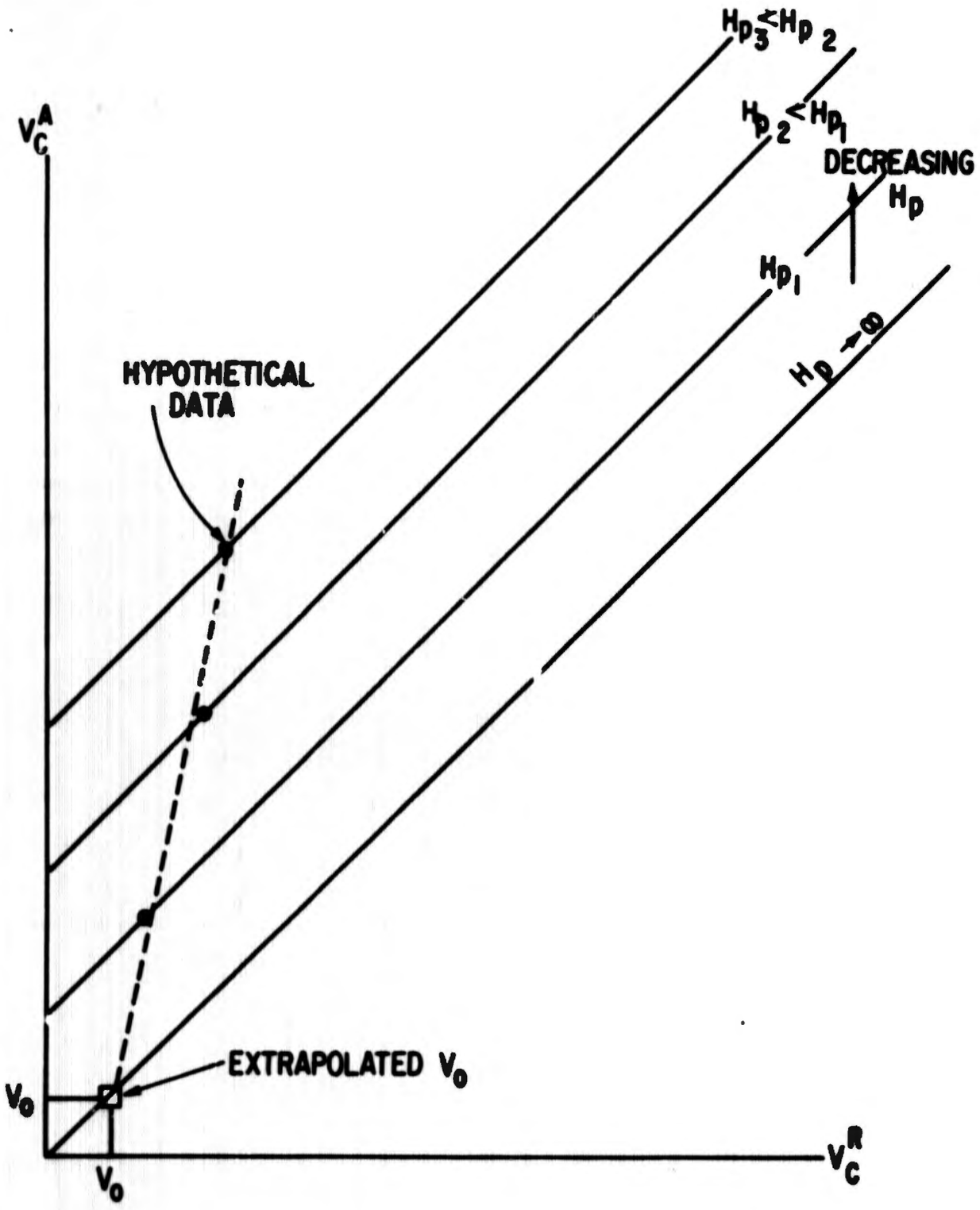

Figure 7. Hypothetical V_C^A versus V_C^R Curve

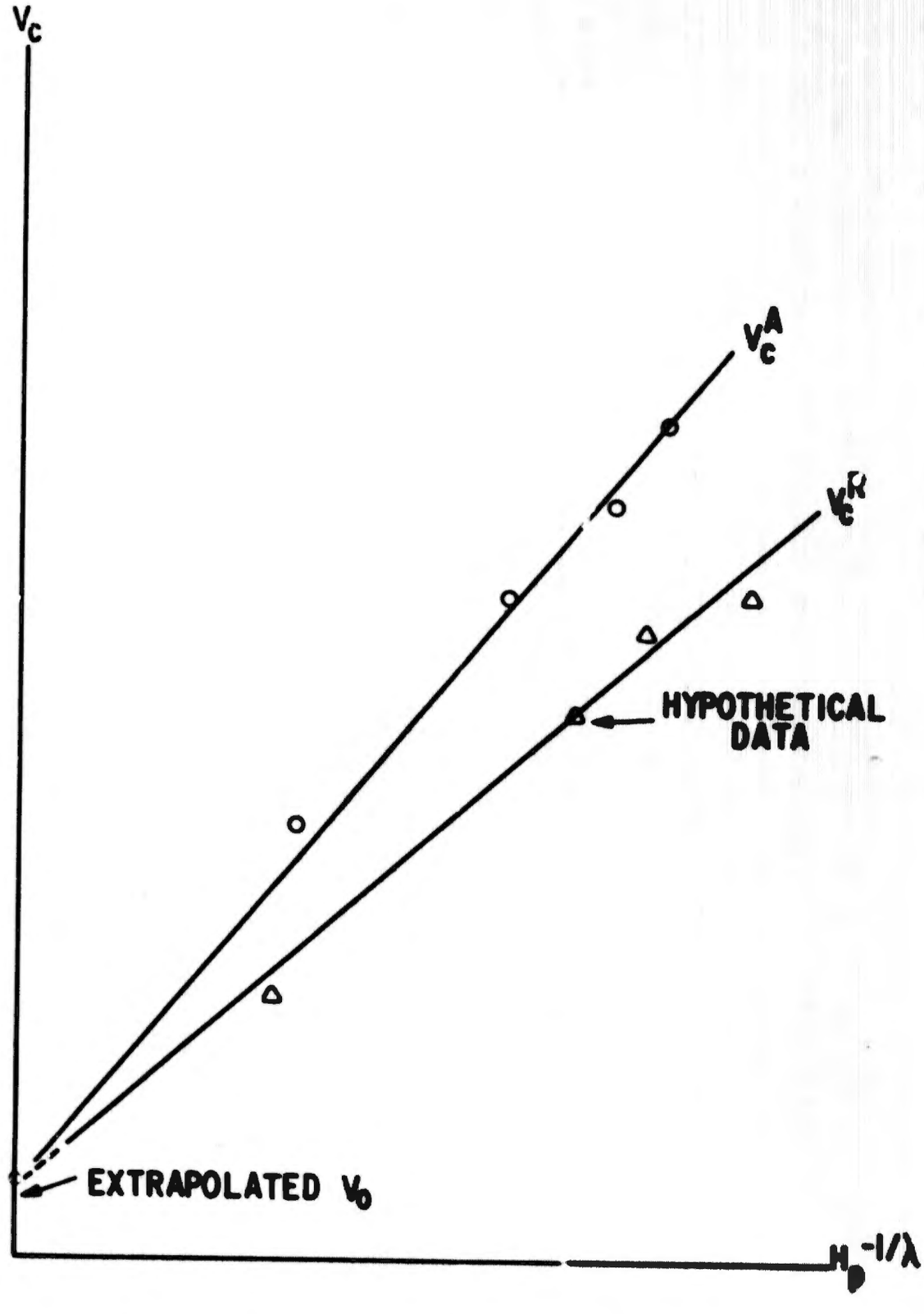

Figure 8. Hypothetical V_C^A, V_C^R versus $H_p^{-1/\lambda}$ Curve

TABLE III

COMPARISON OF IMPULSE VERSUS ENERGY CRITERIA

AIR SHOTS

H_p	V_C^A	$V_C^A H_p$	$V_C^{A^2} H_p$
3.0	2.98	8.94	26.64
5.0	2.13	10.65	22.70
7.5	1.72	12.90	22.20
10.0	1.48	14.80	21.90

VACUUM SHOTS

H_p	V_C^R	$V_C^R H_p$	$V_C^{R^2} H_p$	$T_{max} \Delta t$	$T^2_{max} \Delta t$
5.0	0.98	4.90	4.80	2.14	73.8
7.5	0.84	6.30	5.30	2.89	87.8
10.0	0.65	6.50	4.20	2.74	63.5

STANDARD DEVIATIONS

$V_C^A H_p$	$V_C^{A^2} H_p$	$V_C^R H_p$	$V_C^{R^2} H_p$
6.7	4.9	0.76	0.30

$$\Delta t = \frac{2\bar{H}_p}{U_s^F}$$

or

$$\Delta t = \frac{2\bar{S}_2^R}{U_s^t}$$

The first ratio considers only flyer parameters and is based upon two transit times of a shock wave in the flyer. The second expression considers the relationship between spatial displacement and its corresponding time based on the velocity of a shock wave in the target. The spall depth, $\bar{S}_2^R$, can be either observed or calculated. To calculate an approximate $\bar{S}_2^R$ one can use the above ratios to yield the following expression:

$$\bar{S}_2^R = \bar{H}_p\left(\frac{U_s^t}{U_s^F}\right)$$

These expressions for approximations of Δt and $\bar{S}_2^R$ can be realized graphically by the x - t diagram in Figure 9. The x - t diagram is a position-time history of shock waves in both target and flyer materials. The 10-mil Mylar case is shown completely with the intersections drawn for only the 5- and 7.5-mil flyers. The diagonal lines represent wave or characteristic lines and are drawn with slopes equal to the reciprocals of the shock velocities, corresponding to the different critical flyer velocities and thus different stress levels. For 6061-T6 aluminum there is no significant variation of shock velocity within the stress levels experienced, and thus a common shock velocity of 5.4 mm/μsec can be used to draw target characteristic lines. However, as shown in Table IV, the Mylar shock velocity does change noticeably with the stress levels experienced in this study. Thus values of 3.5, 3.4, and 3.2 mm/μsec were used for the 5-, 7.5-, and 10-mil Mylar flyers, respectively. The regions (A, B, etc.) in the x - t diagram represent constant stress states. Regions A, B, D, and E are states of zero stress. Region C is that of compression and, region F that of tension. The depth, $\bar{S}_2^R$, is that position in the target where tension first occurs in time and then remains under tension for the longest time. The duration of the tension,

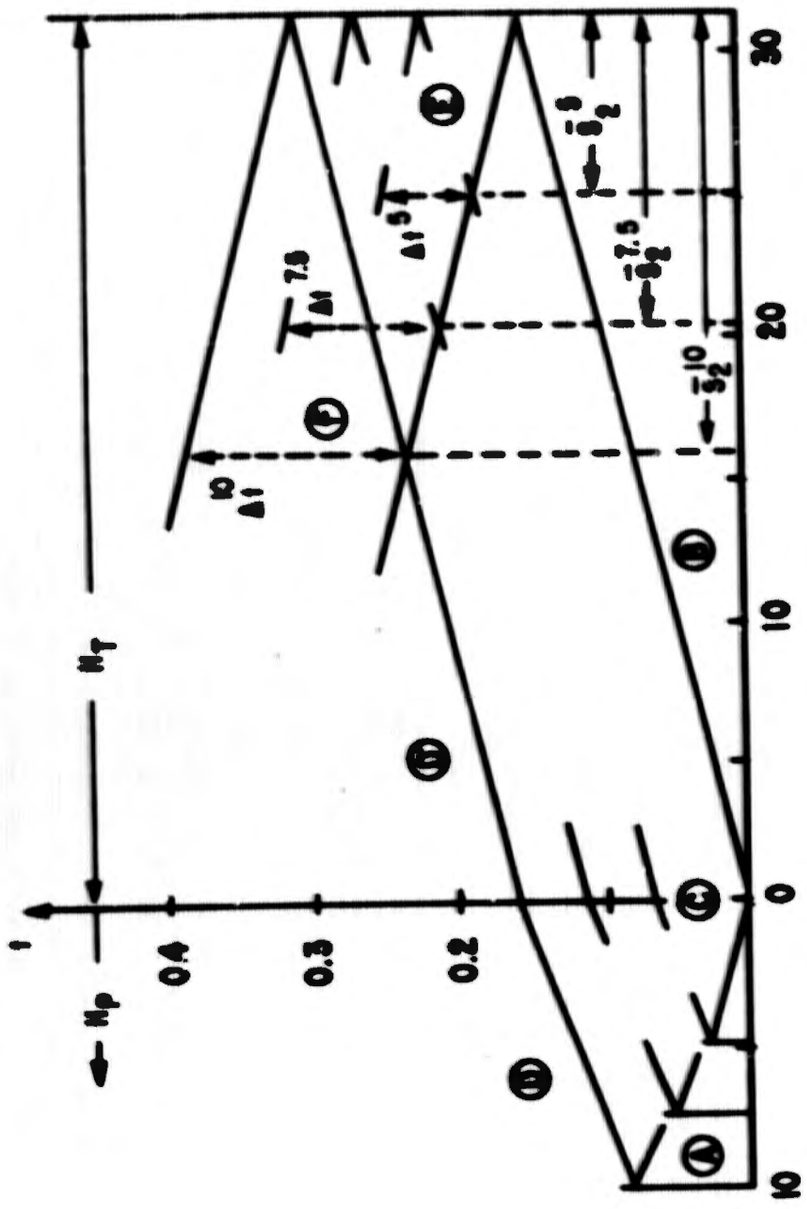

Figure 9. Distance-Time Approximations

Δt, is the time the spall depth is under tension until relieved by a release wave from either the impact or rear free surface. Region D represents the condition when the flyer rebounds away from the impact interface, thus creating a new target free surface and a relief wave propagating toward the target rear free surface.

TABLE IV

MYLAR SHOCK VELOCITY VERSUS PRESSURE

U_s (cm/μsec)	Stress (kb)
0.376	41.2
0.352	36.5
0.346	33.3
0.339	29.6
0.329	27.3
0.315	22.1

The regions on the x - t diagram correspond to points on a σ-Up diagram, as shown in Figure 10. Knowledge of the impact velocity and shock impedances of flyer and target allow the construction of a stress-velocity plot and a means of approximating stress magnitudes. Points A and B describe conditions prior to impact; C is the result of initial impact; D is the flyer rebounding; and F is a condition of rarefaction interaction, and thus tension. Assuming the maximum values of tension to be equal to those values of initial compression, one can calculate the stress levels as follows:

$$T_{max} = \frac{Z_T \quad Z_F}{Z_T + Z_F} V_C^R$$

Table V summarizes the values of Δt, $\bar{S}_2^R$, and T_{max} obtained from the above approximate analysis. Pulse duration Δt^* was determined from a calculated spall depth, whereas Δt^{**} was calculated using an observed value of spall depth. The single calculations are also compared with values derived from the P-PUFF 66 computer code analysis.

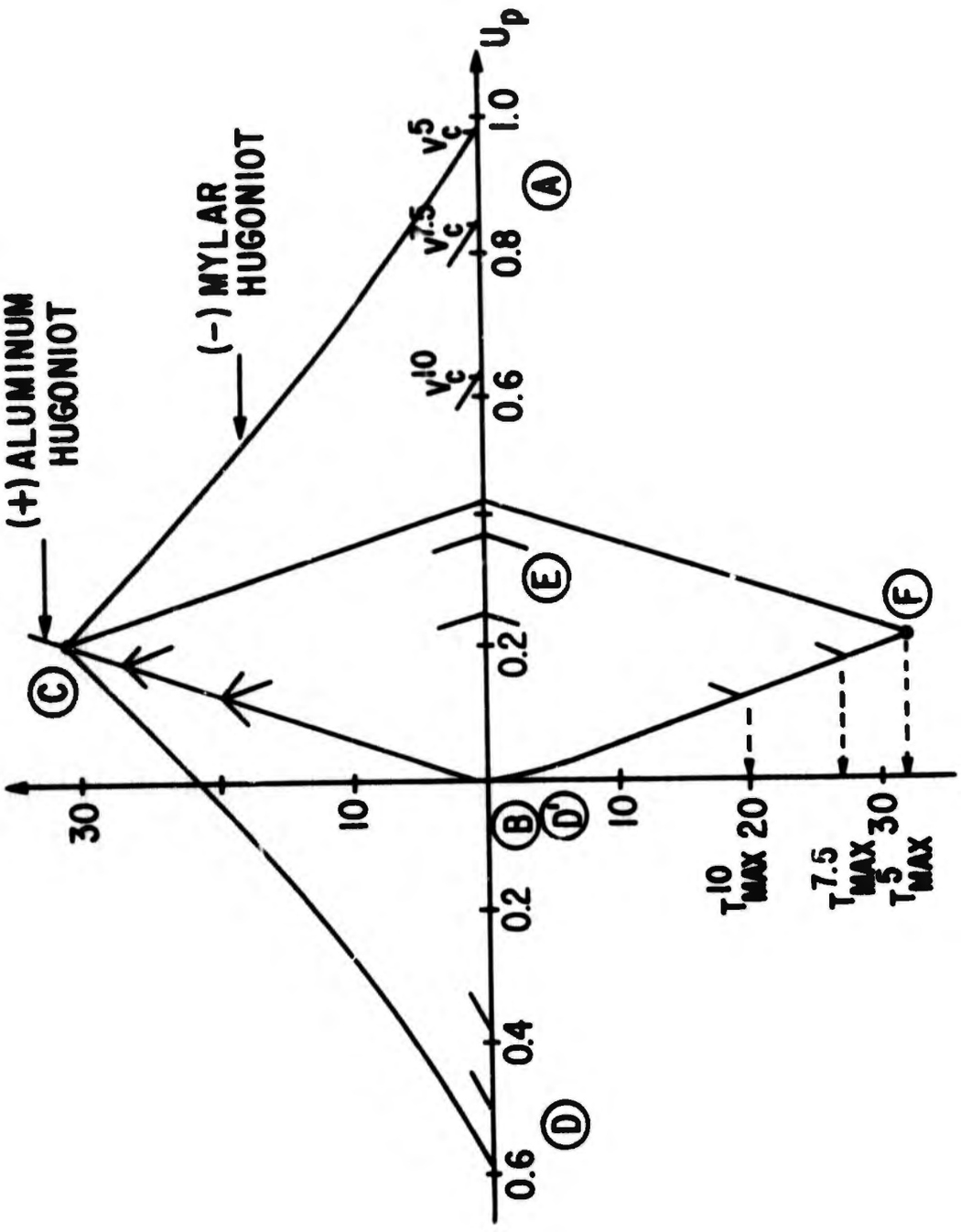

Figure 10. Cross Hugoniot Approximations

TABLE V

COMPARISON OF OBSERVED, P-PUFF, AND APPROXIMATED VALUES

	P-PUFF		Observed	Approximated			
H_p (mils)	Δt (μsec)	Tmax (kb)	$\overline{S}_2^R$ (mils)	$\overline{S}_2^R$ (mils)	Δt^* (μsec)	Δt^{**} (μsec)	Tmax† (kb)
5.0	0.062	34.5	9.3	7.7	0.072	0.088	35.7
7.5	0.095	30.4	12.5	11.9	0.112	0.118	30.0
10.0	0.118	23.2	15.6	16.1	0.159	0.146	22.2

* from calculated value of spall depth
** from observed value of spall depth

† from equation $\text{Tmax} = \frac{Z_T \quad Z_F}{Z_T + Z_F} V_C^R$

8. EFFECT OF AN AIR LAYER

When thin flyer impact experiments are performed with normal atmospheric conditions, a layer or cushion of air of finite thickness is trapped between flyer and target. The commonly accepted assumption is that the induced shock profile is distorted. As a result of the analysis conducted in this report on data produced in both air and vacuum environments, certain general facts are evident. The first fact is that there is a significant difference in what the target experiences when impacted with an air layer as compared to a vacuum environment. The second conclusion is that it is possible to obtain a reasonable estimate of the dynamic material strength of a target by performing impact experiments in air alone.

The effects of an air layer on thin flyer impact experiments can be described as follows:

a. There is no noticeable change in target damage mechanisms between air and vacuum inpacted specimens.

b. Flyer thicknesses in air are equivalent to larger values in vacuum environments, and they approach each other with increasing flyer thickness.

c. Larger critical velocities are required in air to cause equivalent damage in vacuum environments, and they approach each other with increasing flyer thickness.

d. For a given flyer thickness, the spall depth locations as measured from the rear surface are larger in air than in vacuum and they approach each other with increasing flyer thickness.

e. The induced stress profile is lower in amplitude, and approaches vacuum values as flyer thickness increases.

Threshold data produced with the effects of an air layer are useful for estimating the dynamic material constants (λ, k) for a target material. The sections on theory and experimental results derive and employ the analytic expressions which relate vacuum experimental data on critical velocity, spall depth, and flyer thickness with stress and stress duration. The common factors of all of these expressions are the material parameters, λ and k. Uniquely, when one fits the air values of flyer velocity, flyer thickness, and spall depth to the same equation form for the vacuum values, the result yields essentially identical values of λ. The only distinctions are the displacement constants which account for the distorted stress profile caused by the effects of the air layer. Thus, by fitting air-derived values of critical velocity, flyer thickness, and spall depth, one can obtain a reasonable material parameter (λ) measurement which can then be applied to stress and stress duration relationships. The result is a useful approximation of the dynamic strength of a material based entirely on impact data produced in an air environment.

SECTION IV

EXPERIMENTAL TECHNIQUE

1. FLYER PLATE SET-UP

The experiments were performed in the Pulse Power Laboratory of the Air Force Weapons Laboratory. The equipment consisted of a fast discharge capacitor bank, vacuum system, electronic diagnostic equipment, and a high-speed camera (Figure 11), and has been described in detail in several earlier works (Refs. 8 and 9).

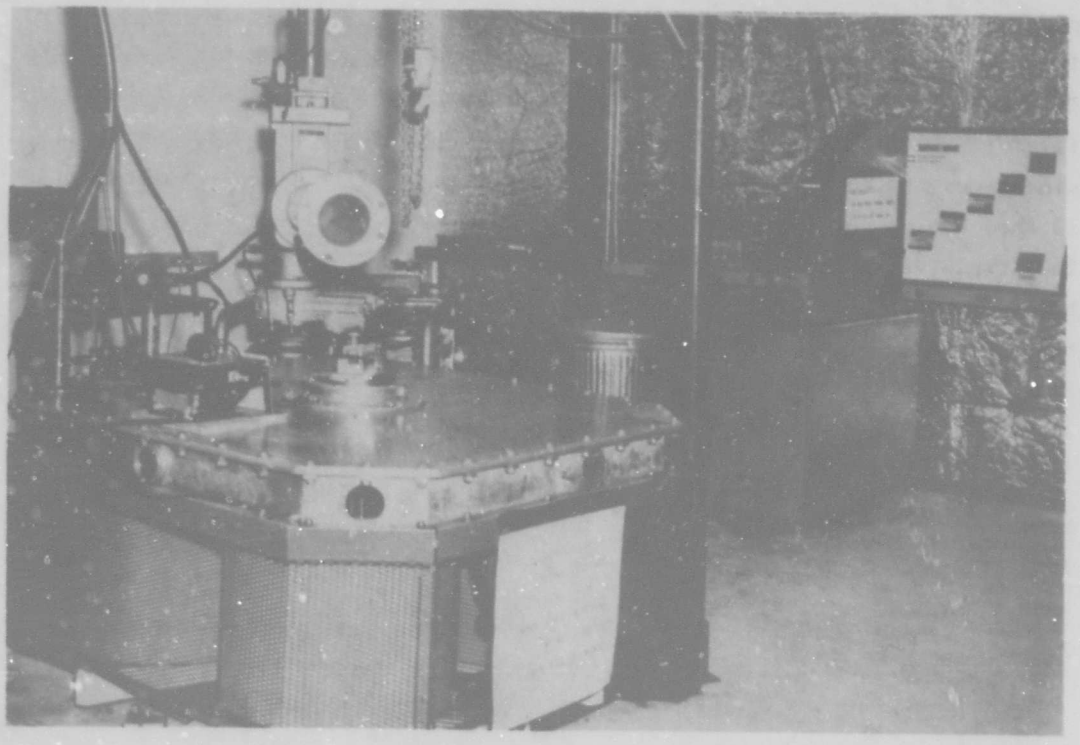

Figure 11. Experimental Apparatus

The capacitor bank used for this study stored a maximum of 16,000 joules for a charged voltage of 125,000 volts. The bank consisted of four 0.5 microfarad capacitors connected in parallel. The energy was dumped into a foil assembly by a nitrogen spark chamber. The partial gas pressure was adjusted to give the desired overvoltage at which arcing occurred and the stored energy was transferred to the foil assembly. The foil undergoes rapid joule heating and vaporization. The flyer plate is accelerated by the expanding vapor.

The foil is an integral part of the exploding foil assembly, specially fabricated for accelerating thin plastic flyer plates. In this study, for accelerating thin plates of Mylar, a type "A" assembly was fabricated as follows.

A lucite block (1/2 x 3 x 3 inches) with a shallow groove through the middle forms the base of the assembly. This is a back-up block and confines the vapor so that it expands against the flyer. Copper electrodes are glued to this block with Eastman 910 adhesive, and a very thin (0.25 mil) aluminum foil is placed across the electrodes. A sheet of either 3-, 5-, 7.5-, or 10-mil Mylar is then glued to the assembly. In this way, the foil is completely enclosed. This ensures a high maximum transfer of energy from the vaporizing foil to the flyer. A Lucite barrel with a centered opening corresponding to the desired dimensions of the flyer was finally bonded on top of the Mylar. Figures 12 and 13 show the pieces and end product which constitute the type "A" foil assembly. The completed foil assembly is placed between the electrodes of the capacitor bank (Figure 14), and the electrodes of the assembly are firmly clamped to the bank terminals. On bank discharge, the expanding aluminum vapor shears the Mylar and accelerates a flyer which is the exact size of the aperture. At late times, the entire assembly breaks under the force of the expanding vapor.

The vacuum experiments were performed in a bell jar which was pumped down, by a combination roughing and diffusion system, to pressures between 10^{-5} and 10^{-6} mm Hg. The air experiments were performed without any container, and the amount, or layer, of air was held constant with a flyer-target separation of 2.0 cm.

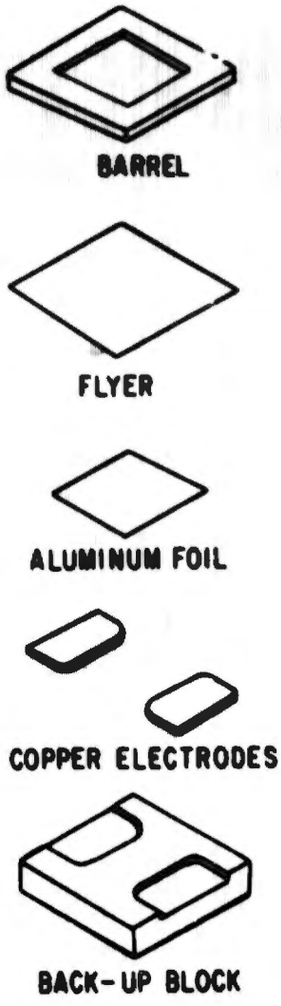

Figure 12. Elements of Exploding Foil Assembly

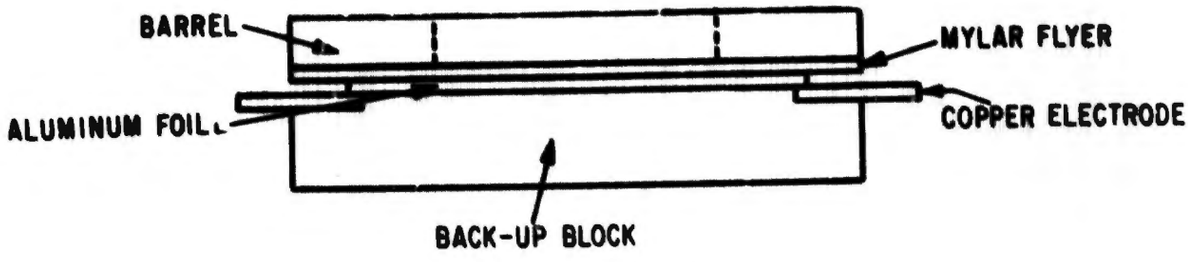

Figure 13. Diagram of Assembled Foil Block

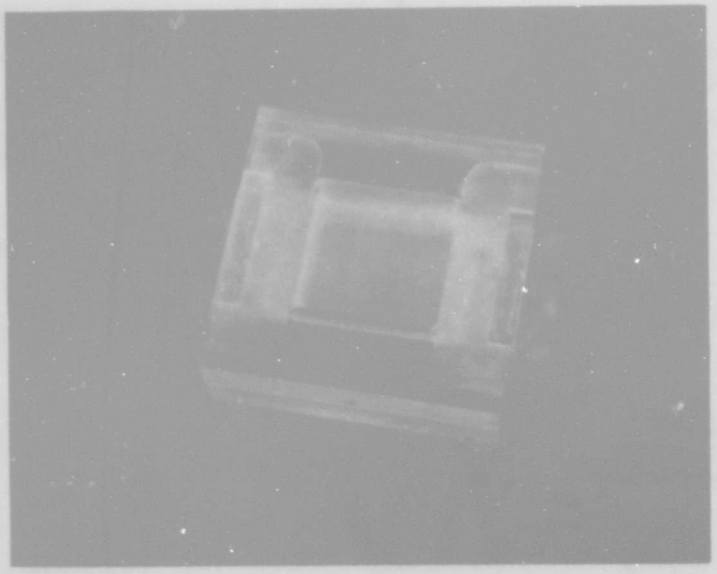

Figure 14. Exploding Foil Assembly

2. DATA REDUCTION

The velocity of the flyer plate was determined by high-speed photographs. A Beckman and Whitley Model 180 framing camera records the flyer plate before impact. The motion of the flyer relative to some fixed point was measured in consecutive frames. Figure 15 is representative of this film record. The velocity of the flyer is simply its displacement divided by the time interval between film frames. These results are then statistically analyzed, poor data records eliminated, and the average velocity and its variance determined. This is done by simple computer calculations. The difficult aspects of data reduction are obtaining enough information to plan the next experiment, and evaluating the value of each experiment. To satisfy these requirements, the following procedure was used:

a. The framing camera film record was processed and the film examined to determine that impact was planar and that an adequate number of frames were available for velocity determination. If either of these requirements was not fulfilled, the experiment was discarded.

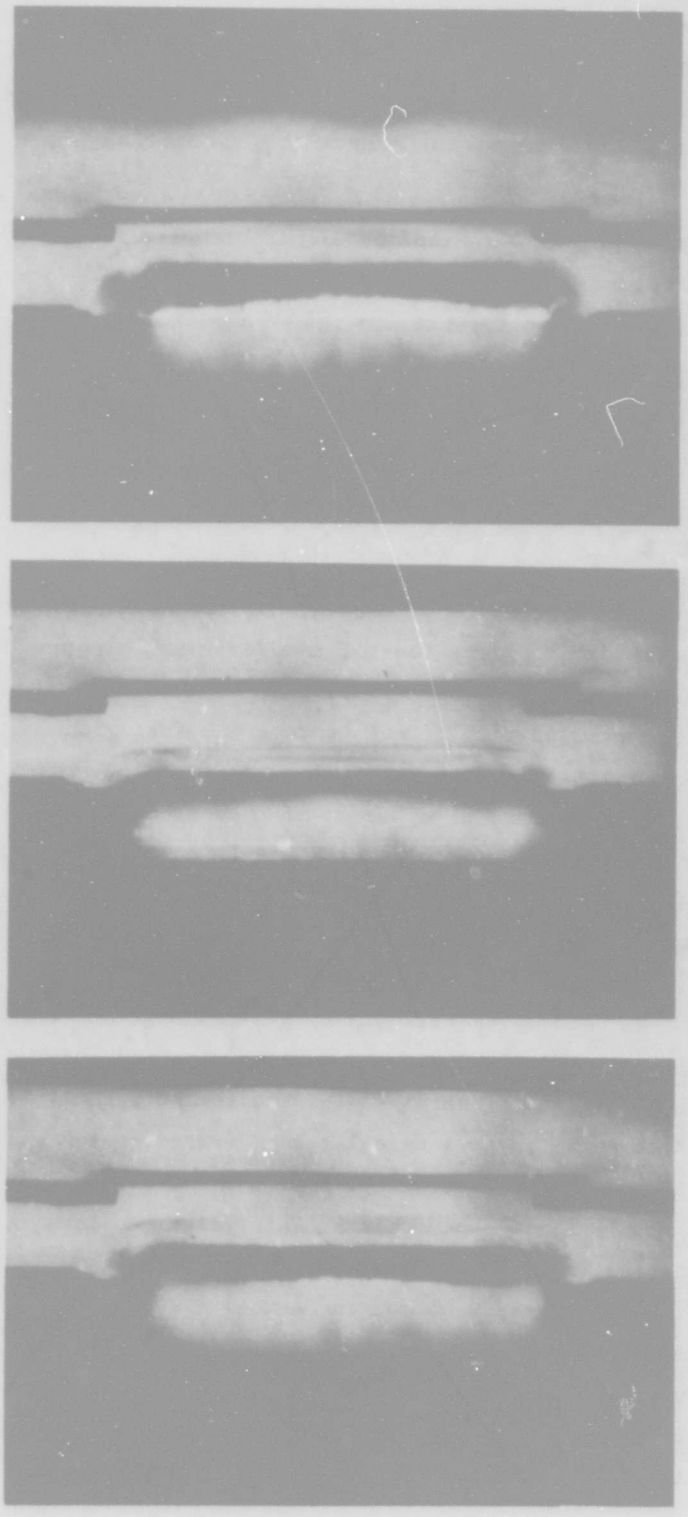

Figure 15. Impact Condition

b. An approximate flyer velocity was calculated to determine if the desired velocity had been obtained. Variations in discharge efficiency, bank discharge voltage, and flyer shear affect the flyer velocity. If the flyer velocity was outside the range of interest to the experiment, no further processing of the experiment was done.

c. The target specimen was examined either visually for obvious failure or optically for incipient failure. If the examination revealed other than one-dimensional damage, the results were ignored.

d. Precise calculations of flyer parameters and of discharge parameters were made. These were used to calculate the pressure-time history and to plan the next experiment.

The final form of each experiment performed is a computer yield output data sheet as shown in Figure 16.

Of the 195 vacuum experiments performed, 43 were discarded because of inadequate flyer velocity data. Forty-four of the remaining were used to determine the critical velocity for incipient spall. The other data were eliminated because of poor impact planarity of the tests. The following criteria were used to eliminate all but the best data. The film records were classified into four groups. Figure 17 gives examples of three of these groups. For this study, only those experiments within the planarity 1(P-1) category were further evaluated. Shots such as P-2, P-3, and P-4 were excluded from further analysis. A criterion was developed to quantitatively evaluate the planarity of the P-1 shots. An approximate time of flyer arrival was calculated from the film record of flyer motion just before impact. Since less than 1/2 centimeter of the target's center was evaluated for damage, only 1/2 centimeter of the center of the flyer was used to calculate planarity. This approximate analysis is demonstrated in Figure 18. A closure time was calculated by measuring the spatial displacement and dividing this by the flyer velocity. Closure times ranged from 100 to over 500 nanoseconds. Only those shots that had arrival times less than 500 nanoseconds were used in the final analysis. The maximum closure time could not be determined since only one camera was used. Also, the actual flyer edges are sometimes undistinguishable from foil vapor clouds. Therefore, the criterion does not eliminate all runs with closure times greater than 500 nanoseconds. It should be pointed out that the inclusion of data having planarity of type P-2 would not have significantly altered the results of the type P-1 data.

AIR FORCE WEAPONS LABORATORY

PULSE POWER LAB / WLRP

SHOT REPORT

MATERIAL CODE	AL 6061 - T6			
SHOT NUMBER	9848		SHOT DATE	3MAY68
TRANSDUCER LOAD CODE	A .25 AL (3/2 X 3/2)17.5 MIL 1/4 MI			
FLYER -MATERIAL				MYLAR
THICKNESS			.01905	CENTIMETER
AREA			14.52	SQ. CM
MASS			.3844	GRAM
VELOCITY	1.253	+OR-	.001	MM/MICROSEC
MOMENTUM			481640.9	DYNE-SEC
MOMENTUM/AREA			33180.37	DYNE-SEC/SQ CM
PULSE WIDTH (2T/C)			.1812	MICROSEC
KINETIC ENERGY			301.83	JOULES
SPECIFIC ENERGY			20.79	JOULES/SQ CM
PLANARITY CODE				P1
TARGET-THICKNESS			.0813	CENTIMETER
AREA			19.76	SQ. CM
MASS				GRAMS
VELOCITY				MM/MICROSEC
MOMENTUM				DYNE-SEC
KINETIC ENERGY				JOULES
MOMENTUM RATIO				
EFFICIENCY			33.54	PERCENT
DAMAGE CODE			SPALL	
BANK -DISCHARGE VOLTAGE			30.00	KILOVOLTS
ENERGY			900.0	JOULES
DELAY			1.20	MICROSEC
ELECTRODE GAP			.61	INCH
GAP PRESSURE				ATMOSPHERE
TARGET-FLYER SEPARATION			10.00	MM
EXPERIMENTAL PRESSURE			4.50E-06	MM HG
CAMERA-B.W 189				
SPEED			7997	RPS
TURBINE			18000	
CALIBRATION FACTOR	10.00MM	=	1808	COUNTS
FILM MAGNIFICATION	1.00MM RULE		=.248	MM FILM
DELAY SETTING			345	DEGREES

COMMENTS

EXCELLENT FILM QUALITY

.6 ND FILTER USED

Figure 16. Computer Compilation of Shot Data

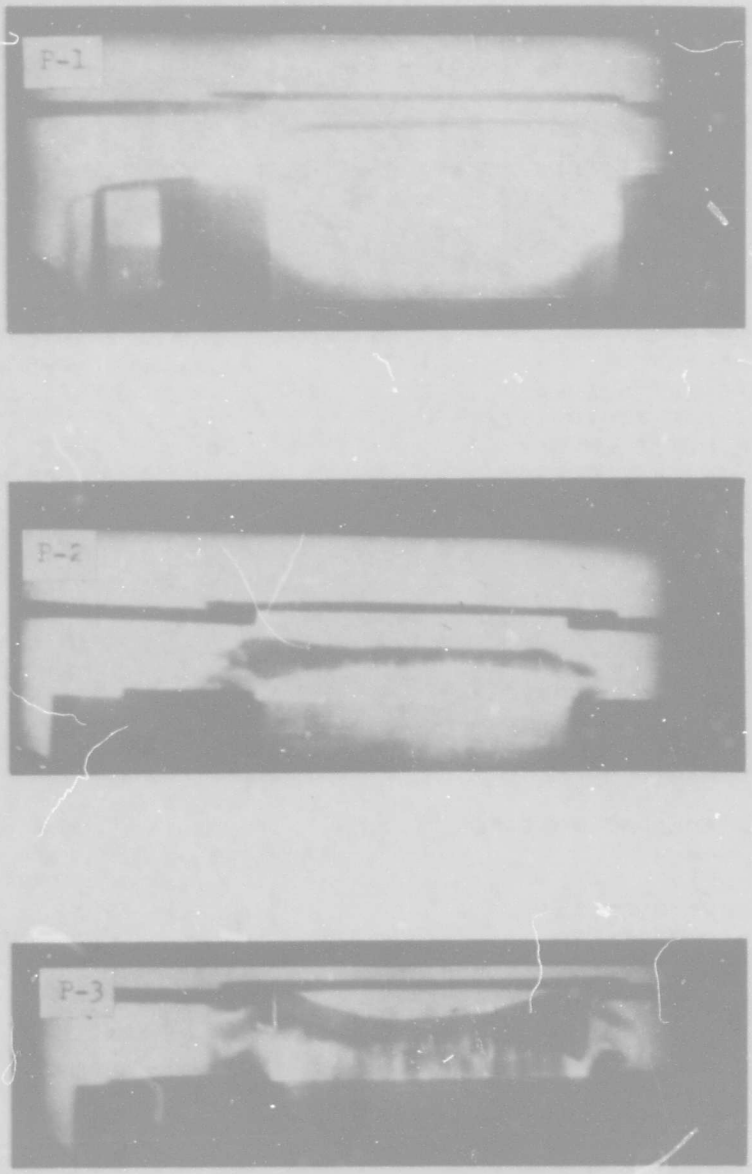

Figure 17. Examples of Planarity

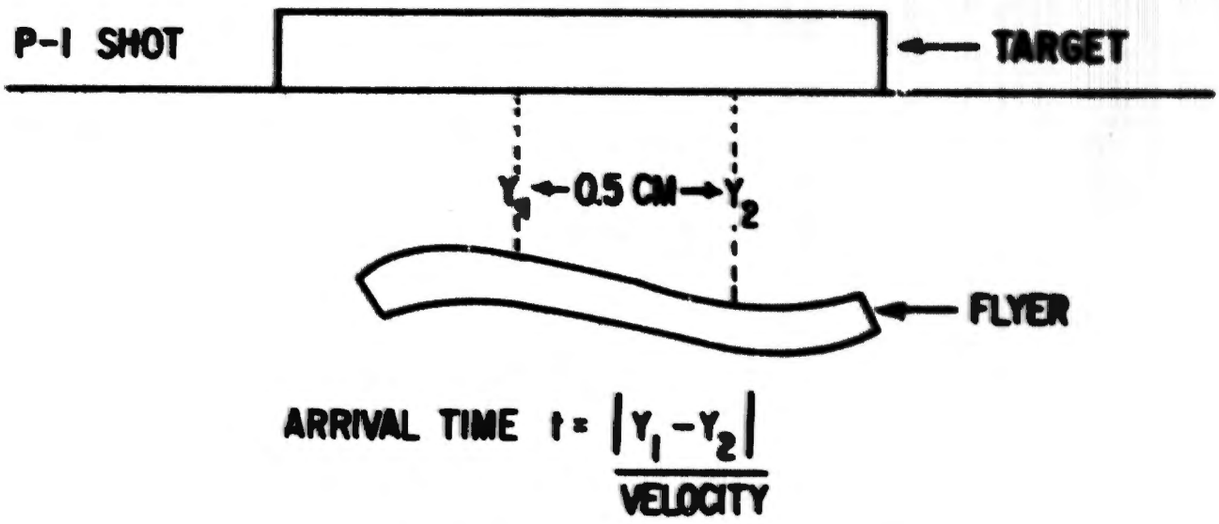

Figure 18. Estimating Flyer Planarity

SECTION V

METALLURGICAL ANALYSIS

The impacted 6061-T6 aluminum targets were examined for both spall depth and extent of damage. A few targets were substantially overdriven (damaged extensively), and the resulting damage was visually discernible. Figure 19 is an example of this gross degree of spall, and clearly shows the effect of momentum being converted into energy to form a spall layer. However, most of the samples had only incipient damage for which the presence of spall could be detected only by internal metallurgical observation, and these conditions are most suitable to study with respect to the determination of a failure criterion. These specimens were sectioned along a center plane transverse to the loading direction. Figure 20 is an example of the metallurgical sectioning.

The prepared samples were viewed at 50x magnification. Figure 21 shows a view of incipient spall.

To obtain measurements of spall depth, grid markings were used perpendicular to the free surface, each covering 7.87 mils between markings, and the depth from the rear surface to the spall area was measured. The error in measuring the depth is approximately $\pm$ 0.5 mm on the photo, or $\pm$ 0.5 mil at unit magnification.

Figure 22 shows such a layout with seven grids indicated. The rear surface corresponds to the free surface of the target, which can usually be recognized by the direction of curvature. Distances are measured from a reference line approximating the rear surface with each grid boundary. This is easily done since the amount of curvature in each incremental length (7.9 mils) is relatively small compared to that over the entire 90-mil distance covered in the photo. Two distances are measured:

a. S_1, the distance from the rear surface to the first sign of spall region.

b. S_3, the distance from the rear surface to the last sign of spall.

If a grid has no observable voids caused by incipient spall, then that grid is not involved in the calculation of the average values of S_1 and S_3 (designated $\overline{S}_1$ and $\overline{S}_3$). These values are calculated by dividing the sum over all of

the grids measured by the total number of usable grids. The distance of the mid plane, $\overline{S}_2$, is calculated by

$$\overline{S}_2 = 1/2\left(\overline{S}_1 + \overline{S}_3\right)$$

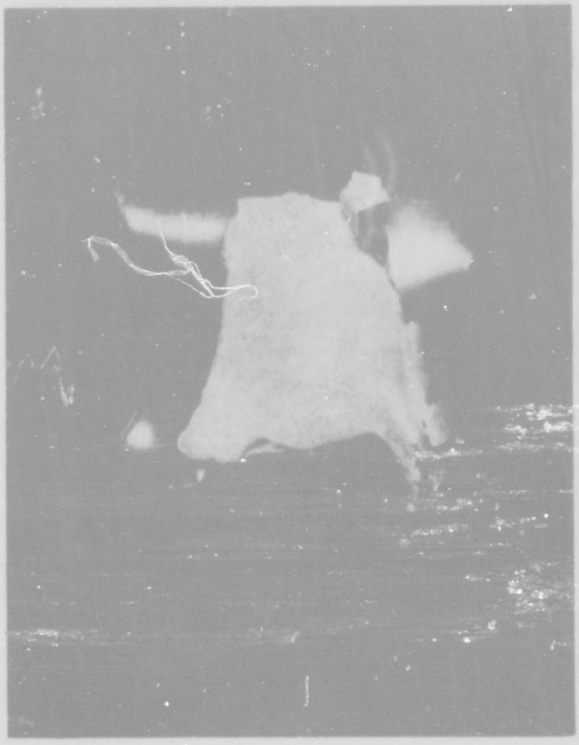

Figure 19. Spalled 6061-T6 Target

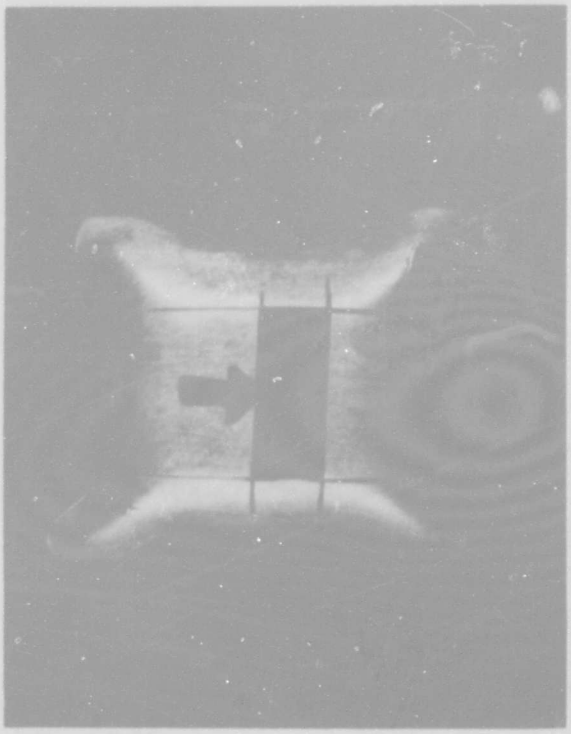

Figure 20. Sectioned 6061-T6 Target

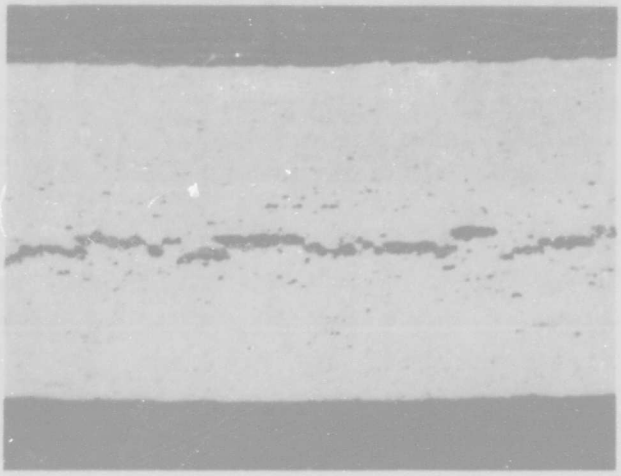

Figure 21. Photomicrograph of Incipient Spall

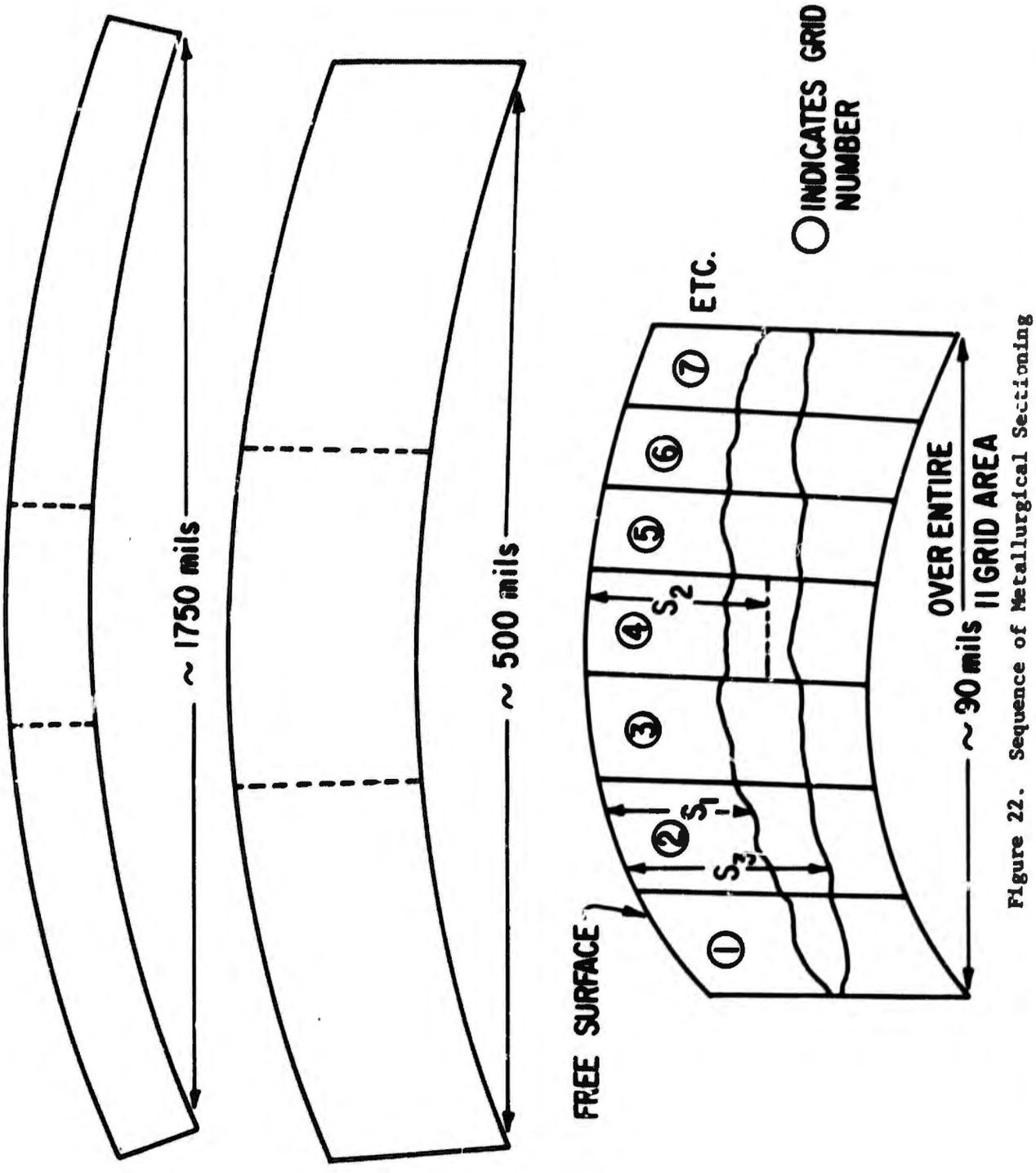

Figure 22. Sequence of Metallurgical Sectioning

SECTION VI

EXPERIMENTAL RESULTS

In this section the results of the measurements of spall depth and critical velocity for spall for the air and vacuum shots are presented. Only the averages for each given flyer thickness are tabulated.

It should be mentioned that the values of $\bar{S}_1$* are included for comparison purposes only, since the stress-time profiles for each flyer thickness were obtained using the P-PUFF code at the distances $\bar{S}_2$*. The critical velocity for spall for a given flyer thickness is that velocity above which damage is assured, and below which no damage results, when examined at 50x magnification.

1. SPALL DEPTH RESULTS

The only damaged shots evaluated for spall depth were those that had good planarity upon impact (P1), thus reducing possible effects caused by specimen distortion. The values of $\bar{S}_1$ and $\bar{S}_3$ were averaged for all shots of a given flyer thickness and values of $\bar{S}_2$ were computed. This was done for both the air and vacuum (reference) shots. The results are shown in Table VI $\left(\bar{S}_2 = 1/2\left(\bar{S}_1 + \bar{S}_3\right)\right.$ for each shot$\left.\right)$.

It was anticipated that the values of $\bar{S}_2$ may depend on the velocities of each individual shot as well as on the flyer thickness (both stress and time dependence). It is possible to relate $\bar{S}_2$ only as a function of H_p for the existing shots once it has been shown that $\bar{S}_2$ does not change significantly over the existing velocity ranges for a constant H_p.

Figures 23 and 24 show plots of $\bar{S}_2$ for both air and vacuum as a function of actual impact velocity for each flyer thickness. It is seen that there is not a significant trend for each flyer thickness, which indicates that the changes are just experimental variation, not functionally related.

---

* For an explanation of these symbols see preceding section.

TABLE VI

SPALL DEPTHS

A. AIR SHOTS - $\bar{S}_2$

3.0 mil	$\bar{S}_2$ = 10.33 mil	*d = 1.060 mil
5.0 mil	$\bar{S}_2$ = 11.43 mil	d = 1.202 mil
7.5 mil	$\bar{S}_2$ = 15.12 mil	d = 1.521 mil
10.0 mil	$\bar{S}_2$ = 16.62 mil	d = 1.602 mil

3.0 mil	range = 8.98 - 11.87 mil	5 shots
5.0 mil	range = 9.47 - 13.15 mil	8 shots
7.5 mil	range = 12.76 - 17.89 mil	9 shots
10.0 mil	range = 14.80 - 19.70 mil	7 shots

*M = 1.933

C = 0.950

B. AIR SHOTS - $\bar{S}_1$

3.0 mil	$\bar{S}_1$ = 6.98 mil	d = 0.237 mil
5.0 mil	$\bar{S}_1$ = 8.83 mil	d = 1.504 mil
7.5 mil	$\bar{S}_1$ = 11.23 mil	d = 1.785 mil
10.0 mil	$\bar{S}_1$ = 12.67 mil	d = 1.821 mil

3.0 mil	range = 6.62 - 7.23 mil	5 shots
5.0 mil	range = 7.02 - 11.73 mil	8 shots
7.5 mil	range = 9.02 - 15.00 mil	9 shots
10.0 mil	range = 9.84 - 15.43 mil	7 shots

M = 1.453

C = 0.957

TABLE VI (Cont'd)

C. VACUUM SHOTS - $\bar{S}_2$

5.0 mil	$\bar{S}_2$ = 9.32 mil	d = 0.290 mil
7.5 mil	$\bar{S}_2$ = 12.48 mil	d = 1.408 mil
10.0 mil	$\bar{S}_2$ = 15.63 mil	d = 1.730 mil

5.0 mil	range = 8.88 - 9.63 mil	6 shots
7.5 mil	range = 9.18 - 14.97 mil	19 shots
10.0 mil	range = 13.13 - 18.70 mil	7 shots

M = 1.636

C = 0.994

D. VACUUM SHOTS - $\bar{S}_1$

5.0 mil	$\bar{S}_1$ = 7.16 mil	d = 1.190 mil
7.5 mil	$\bar{S}_1$ = 10.07 mil	d = 1.000 mil
10.0 mil	$\bar{S}_1$ = 13.72 mil	d = 1.082 mil

5.0 mil	range = 5.91 - 9.61 mil	11 shots
7.5 mil	range = 7.87 - 12.06 mil	20 shots
10.0 mil	range = 11.57 - 15.16 mil	8 shots

M = 1.380

C = 0.980

*Symbols: d = standard deviation

M = best fit slope of line passing through origin and least squares fitting of points on $\bar{S}_2 - H_p$ or $\bar{S}_1 - H_p$ plane

C = correlation coefficient

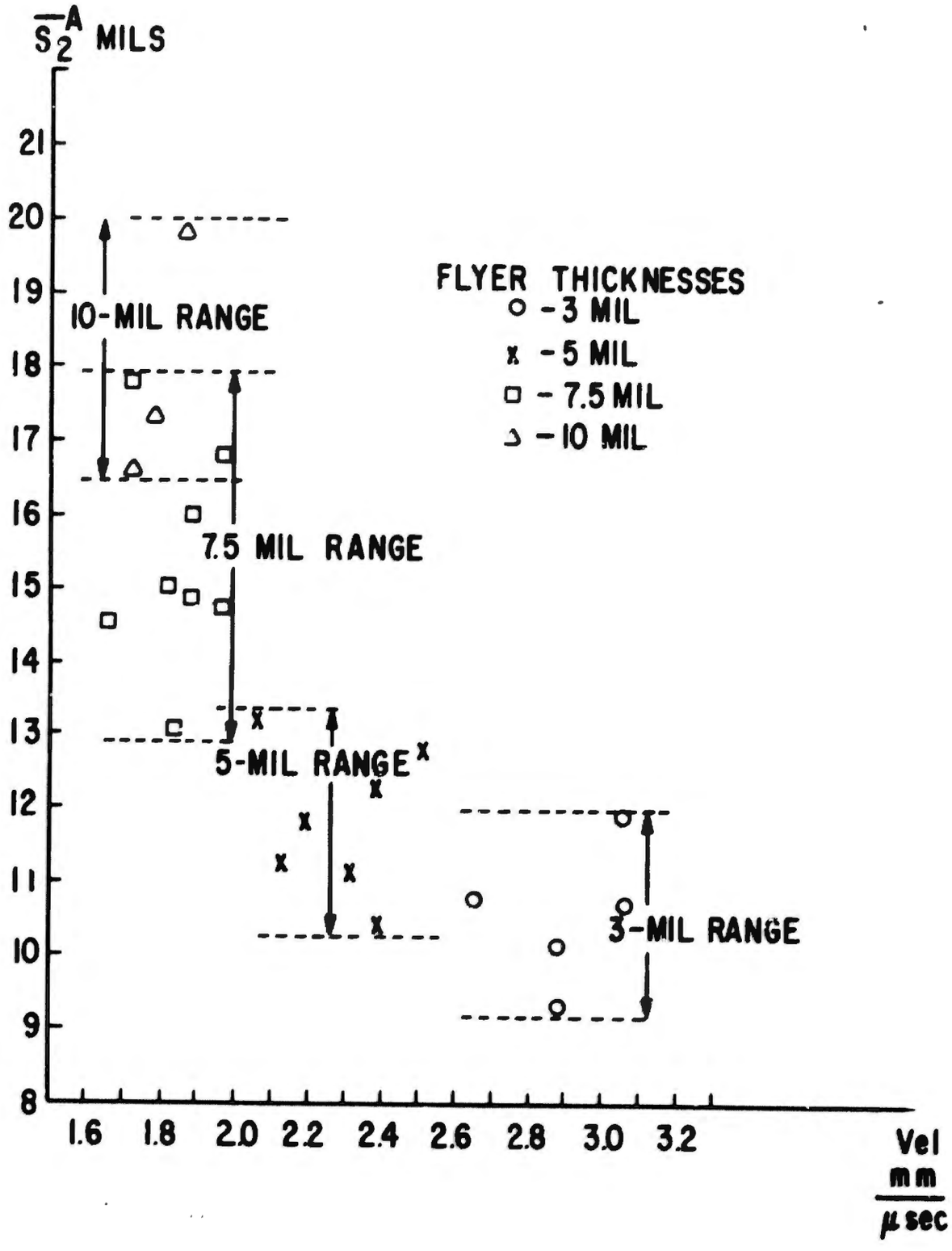

Figure 23. $\overline{S}_2^A$ versus Impact Velocity

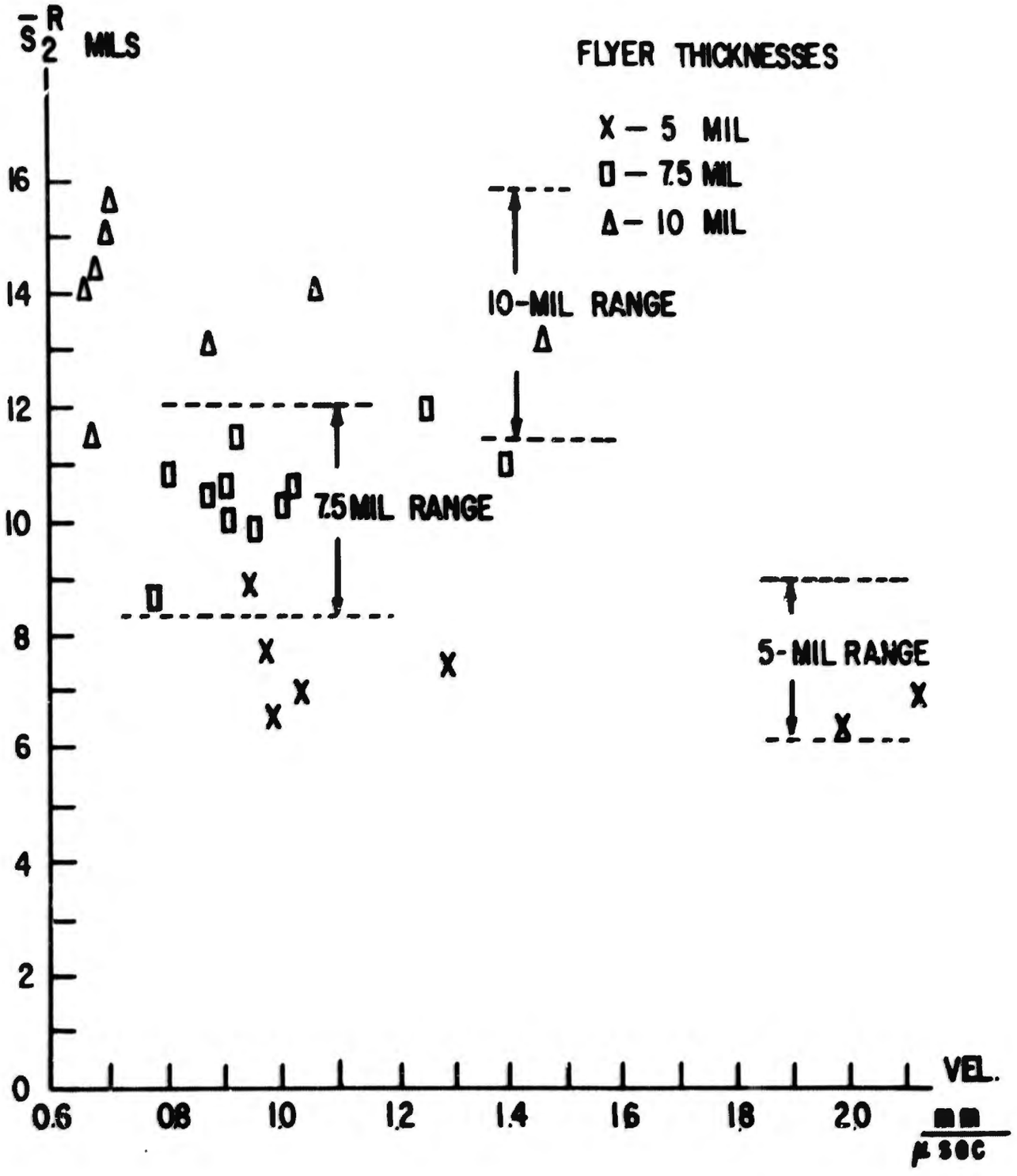

Figure 24. $\bar{S}_2^R$ versus Impact Velocity

2. FLYER PLATE RESULTS

Direct experimental results were obtained for the critical velocity for spall in both air and vacuum. The critical velocity was defined as the velocity that gave observable damage when examined at 50x magnification. In this section the following symbols will be used:

V_c^A, V_c^R = the critical velocities for spall in air and vacuum, respectively, for a given flyer thickness, mm/μsec

H_p = flyer thickness, mils

H_t = target thickness, mils

Tmax = magnitude of first tensile pulse produced at spall plane (spall stress)

Δt = pulse width of above profile measured at a stress equal to 1/2 T_{max}

λ, k, σ_o = parameters in failure criterion suggested by Tuler and Butcher at Sandia Corporation (Ref. 5). This equation relates T_{max} and Δt in the following fashion:

$$Tmax = \sigma_o + \left(\frac{K}{\Delta t}\right)^{1/\lambda} = \sigma_o + K^{1/\lambda}\ \Delta t^{-1/\lambda}$$

These quantities were derived on the basis of stress in kilobars and pulse duration in microseconds. For the P-PUFF hydrocode the units are in dynes/cm^2 and seconds, so that when the values of σ_o, K, and λ are inserted for spall predictions, the value of K must be modified. This new value is designated as K1.

Table VII gives the values of critical velocity in air and vacuum as a function of flyer thickness. The general relation of V_c as a function of H_p can be written as

$$V_c^A = V_o + S_A\ H_p^{-1/\lambda}$$

$$V_c^R = V_o + S_R\ H_p^{-1/\lambda}$$

where S_A, S_R, V_o = material constants. If one does a least-squares fit between the quantity $\left(V_c^A - V_c^R\right)$ for the 5.0, 7.5, and 10.0 mil flyers as a function of H_p, the following values of λ and ψ $\left(\psi = S_A - S_R\right)$ were found to give the optimum fit:

$$\lambda = 1.98$$

$$\psi = S_A - S_R = 2.56$$

SS = sum of squares of deviations in the least-squares analysis = 3.15×10^{-3}.

TABLE VII

CRITICAL VELOCITY VALUES

Flyer material is Mylar: Target: 32-mil 6061T6 Al

H_p (mils)	V_c^A (mm/sec)	V_c^R (mm/sec)
3.0	2.98	---
5.0	2.13	0.98
7.5	1.72	0.84
10.0	1.48	0.65

Table VIII gives the average spall depths versus flyer thickness for the air and vacuum shots. Figure 25* shows these results graphically. The values given correspond to $\bar{S}_2^A$ and $\bar{S}_2^R$ defined as follows:

$\bar{S}_2^A$: The average location of the mid-plane of the spall region as measured from the target rear surface for the air shots.

$\bar{S}_2^R$: The same quantity measured for the shots performed in a vacuum.

---

* M = slope
  B = intercept

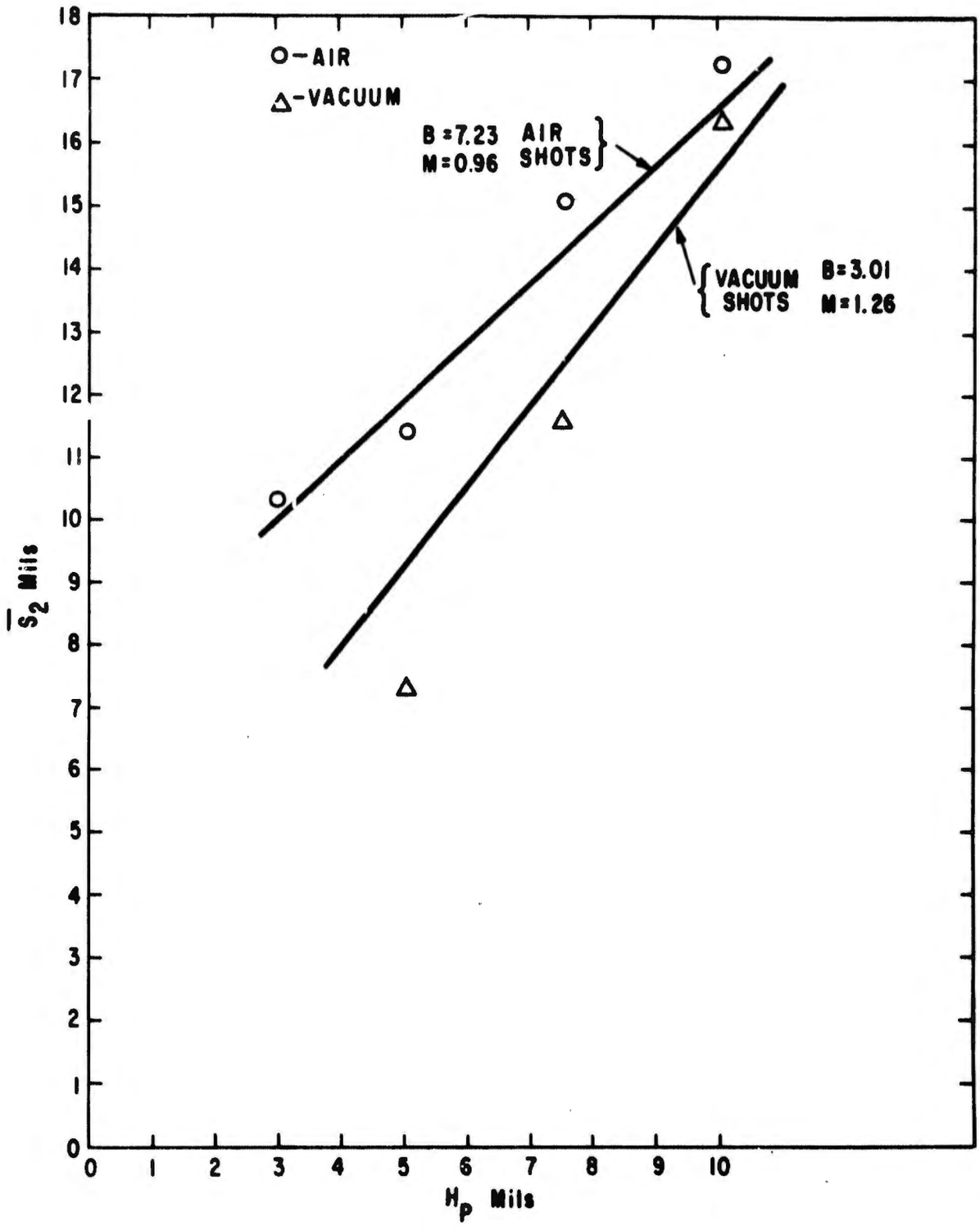

Figure 25. $\overline{S}_2{}^A$, $\overline{S}_2{}^R$ versus Flyer Thickness

TABLE VIII

AVERAGE SPALL DEPTHS

H_p (mils)	$\bar{S}_1^A$ (mils)	$\bar{S}_2^A$ (mils)	$\bar{S}_1^R$ (mils)	$\bar{S}_2^R$ (mils)
3.0	7.0	10.3	---	---
5.0	8.8	11.4	7.2	9.3
7.5	11.3	15.1	10.1	12.5
10.0	12.7	16.6	13.7	15.6

The values for air are consistently higher than those for vacuum (for a discussion on these results and the derivation of all the equations used for the experimental analysis, cf. Section III). A least-squares linear fit gives

$$\bar{S}_2^A = 0.96\ H_p + 7.23$$

$$\bar{S}_2^R = 1.26\ H_p + 3.01$$

These equations are approximately valid, of course, only within the experimentally observed range. If one fits equations of the form, $\bar{S}_2 = \dot{M}\ H_p$, then the following best fit slopes M, are obtained.

Air:

$$\bar{S}_2^A = 1.93\ H_p$$

Vacuum:

$$\bar{S}_2^R = 1.64\ H_p$$

Table IX gives the values of Tmax and Δt as given by the P-PUFF 66 computer code using the critical velocities for spall in a vacuum as the flyer velocity for each flyer thickness.

Figures 26 through 28 show the stress-time edits generated by the P-PUFF hydrocode. Table X enumerates how closely the spall zone location in P-PUFF corresponds with the measured distances. The agreement is well within the

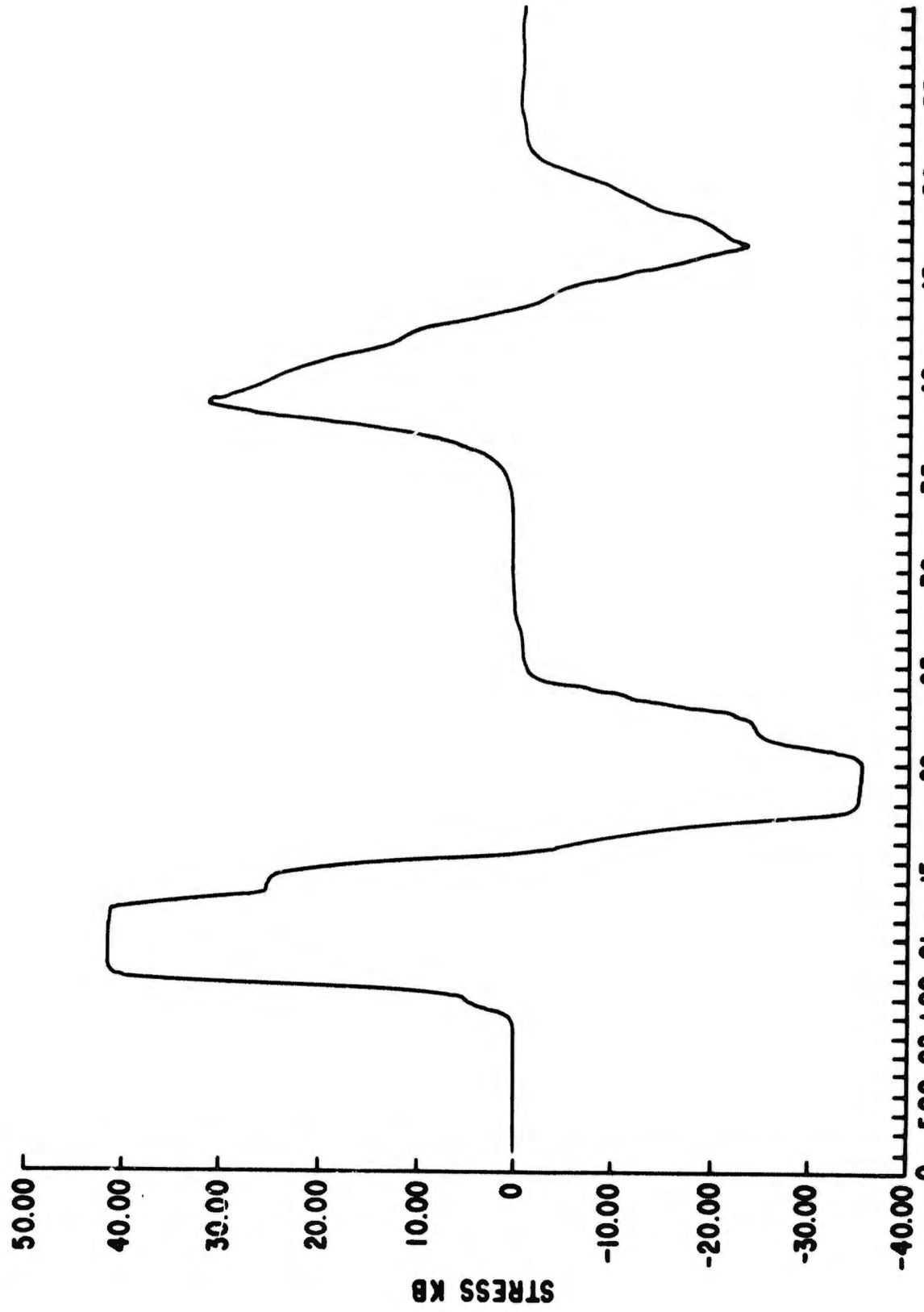

Figure 26. Stress-time Profile at $\bar{S}_2^R$, 5 mil Flyer

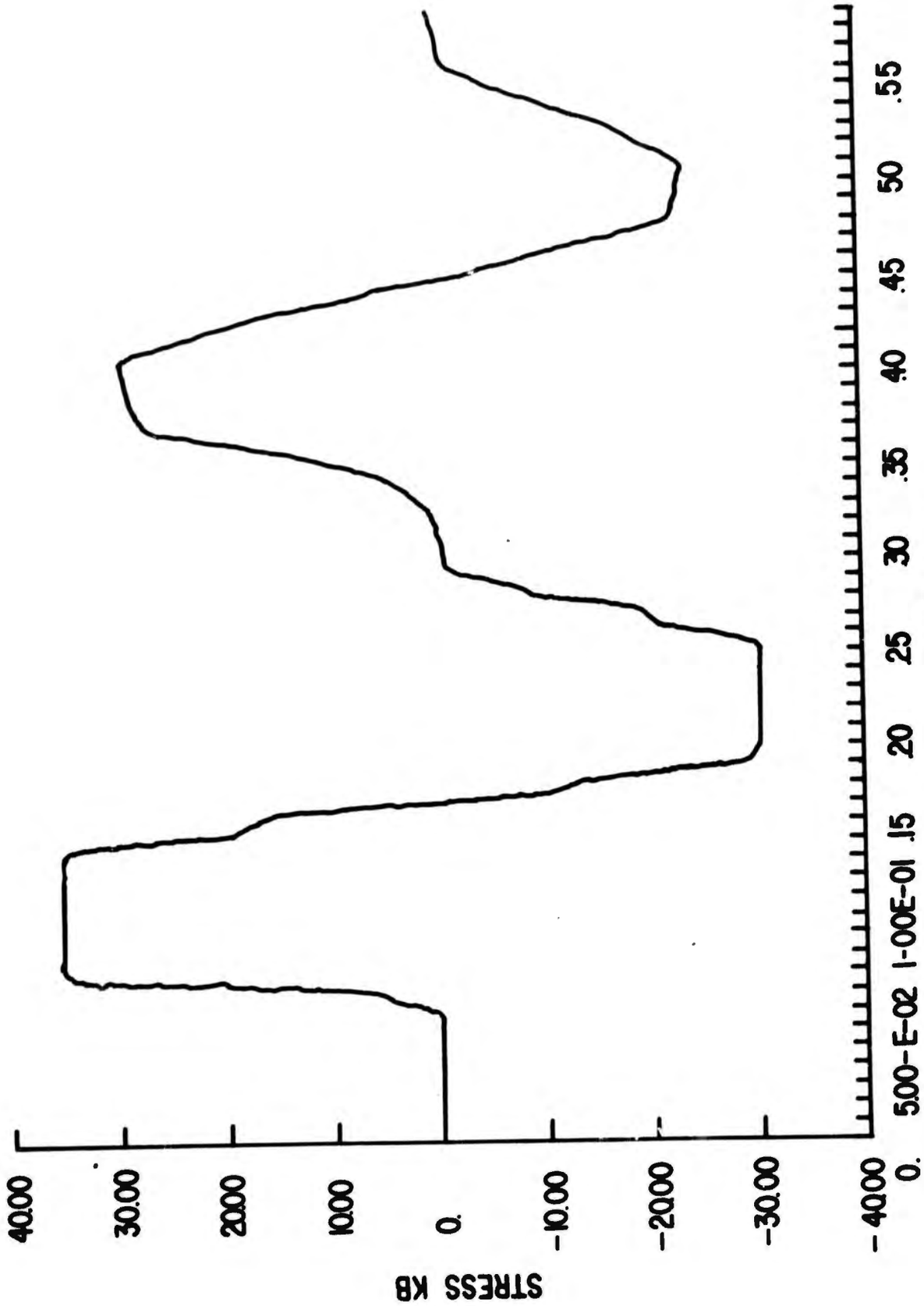

Figure 27. Stress-time Profile at $\bar{S}_2^R$, 7.5 mil Flyer

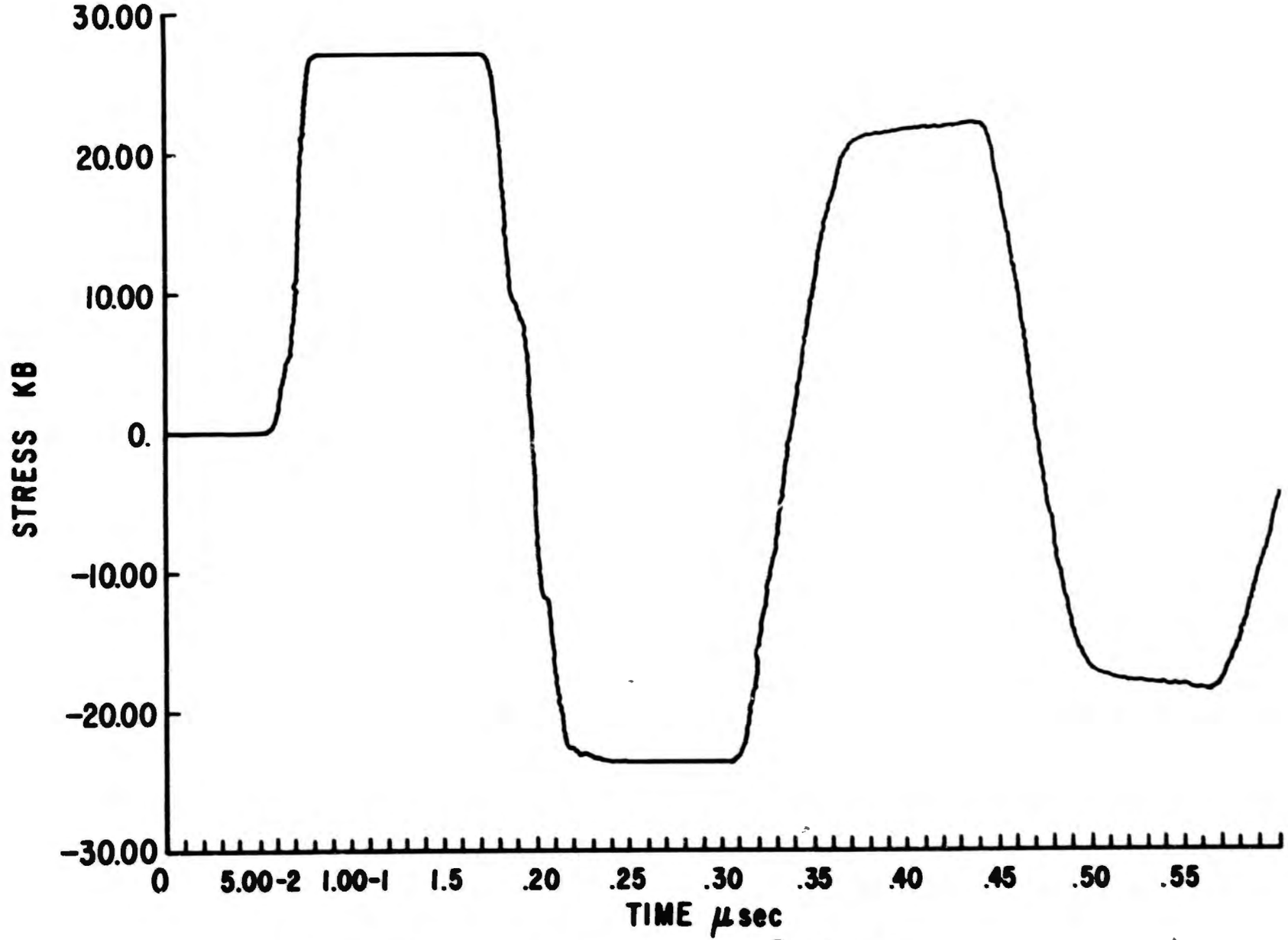

Figure 28. Stress-time Profile at $\bar{S}_2^R$, 10 mil Flyer

TABLE IX

P-PUFF RESULTS

H_p (mils)	V_c^R (mm/μsec)	Tmax (kb)	Δt @ Zero Stress	Δt @ Half Tmax	Δt @ Tmax
5.0	0.98	34.5	0.089	0.063	0.020
7.5	0.89	30.4	0.116	0.095	0.051
10.0	0.65	23.2	0.132	0.118	0.084

TABLE X

P-PUFF EDIT LOCATION VERSUS ACTUAL SPALL DISTANCES

H_p (mils)	S_2 (mils)	Dist in P-PUFF (mils)
5.0	9.3	9.1
7.5	12.5	12.3
10.0	15.6	15.9

experimental error of the depth measurements. (It should be reemphasized that these values of $\bar{S}_2$ are input to the code; once the values of λ, K1, and σ_o have been input, the code can then be used to predict spall location.) The zoning employed in the P-PUFF runs was as follows:

a. Constant zone size in the flyer width = 1.95×10^{-4} cm.

b.* A rezone ratio of 2.36 was used for the first zone in the target. This was calculated on the basis of equal transit times for this zone and the last zone in the flyer.

c. A rezone ratio of 1.00 was used for the remainder of the target giving a zone size of 4.602×10^{-4} cm.

The values of Tmax and Δt were used to determine best fit values of λ and K (K1) by stepping up λ in increments of 0.01 and for each value calculating the best fit value of A satisfying the equation

$$Tmax = \sigma_o + A\,\Delta t^{-1/\lambda}$$

for the data given in Table IX for the vacuum shots. The sum of the squares of the deviations was then calculated (SS) and the value of λ chosen was that one which yielded a minimum value of SS. The results were

$$\lambda = 1.80$$
$$K = 34.9019$$
$$K1 = 5.53158 \times 10^{11}$$
$$SS = 9.31349$$

where K was calculated by $K = A^{\lambda}$. This is in fairly good agreement with the value $\lambda = 1.98$ based on the critical velocity data. Figure 29 shows a plot of Tmax versus Δt based on the vacuum shots.

To check each set of velocity data independently, equations of the form

$$V_c^{\,A} = V_o + S_A\, H_p^{-1/2}$$

$$V_c^{\,R} = V_o + S_R\, H_p^{-1/2}$$

---

* Rezone ratio is the ratio of the size of any zone to the one preceding it (cf. Ref. 3).

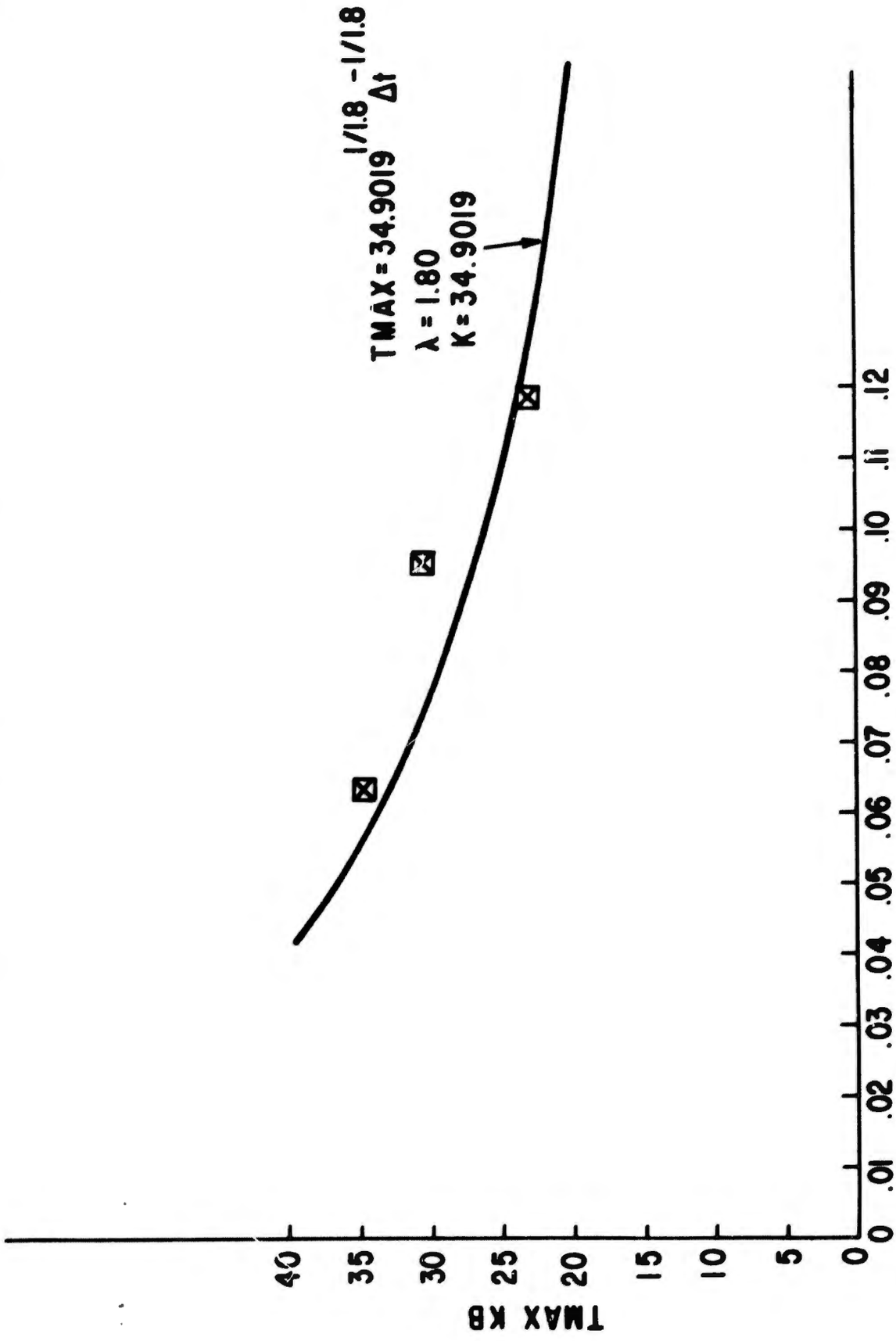

Figure 29. T_{max} versus Δt - Vacuum Data

were fitted in the least-squares sense to the data sets for the vacuum and air shots. Figure 30 shows V_c^A and V_c^R as functions of flyer thickness. The results of the numerical analysis above will be as follows:

Vacuum	Air
$V_o = -0.11$	$V_o = -0.41$
$S_R = 2.46$	$S_A = 5.79$
$SS = 2.6062X10^{-3}$	$SS = 6.81697X10^{-3}$

A further analysis was performed by utilizing a value of $V_o = 0.0$ in the same form of analysis used before: stepping up the value of λ and finding that value which gave a minimum SS. Thus, equations of the form

$$V_c^A = S_A H_p^{-1/\lambda}$$

$$V_c^R = S_R H_p^{-1/\lambda}$$

were fitted to each set of critical spall velocity data. The results were

Vacuum Shots Three Flyer Thicknesses	Air Shots Four Flyer Thicknesses
$S_A = 2.4087$	$S_A = 5.6617$
$\lambda = 1.82$	$\lambda = 1.69$
$SS = 3.02759X10^{-3}$	$SS = 4.50347X10^{-3}$

This routine was followed because only two parameters can adequately be determined at a time. The important factors are that the equational forms fit the data very well in both cases and that both yield a value of λ closer to 2.0 than to 1.0.

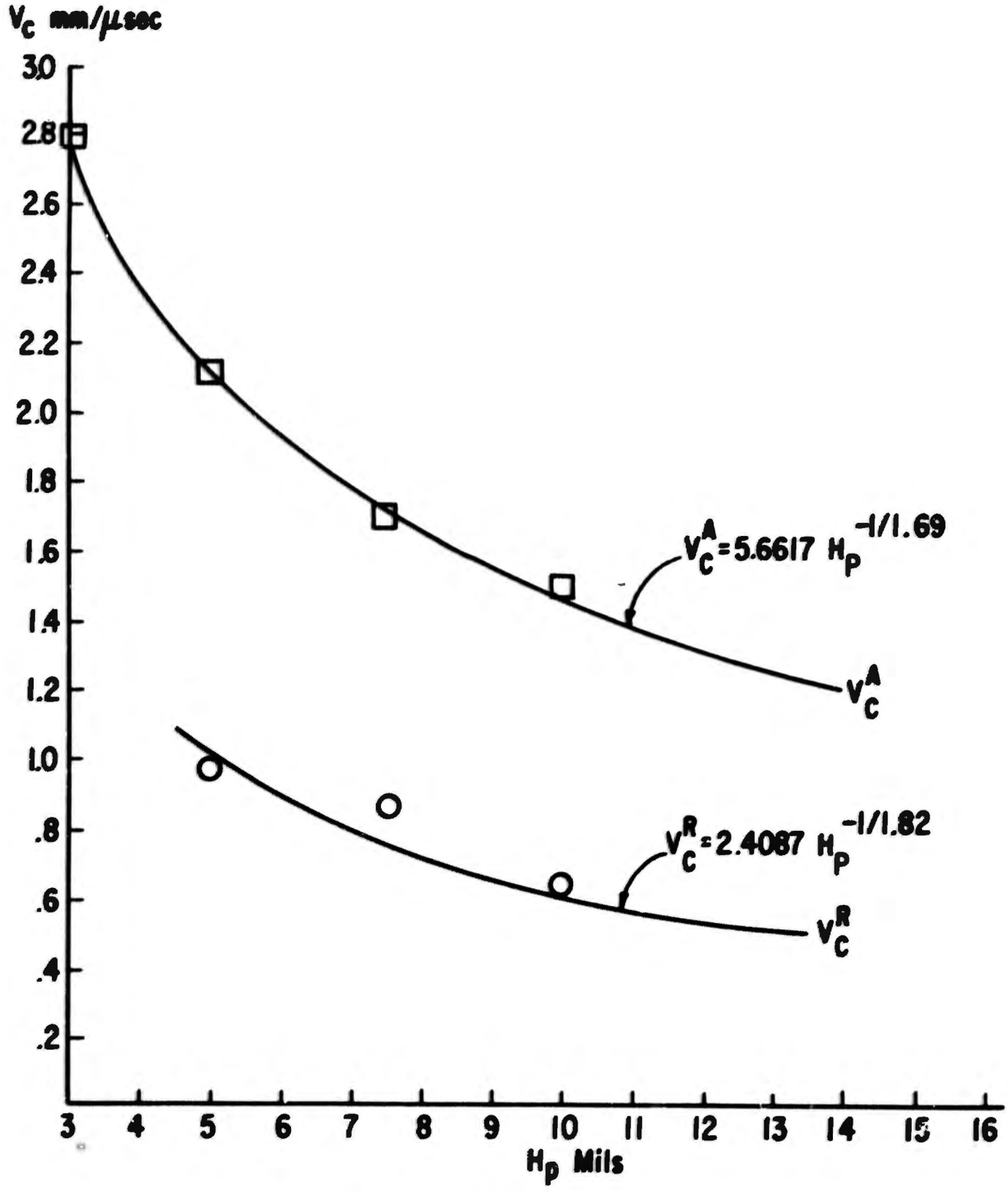

Figure 30. V_c^A, V_c^R versus Flyer Thickness

The values of V_o calculated before were less than zero, which obviously has no physical significance. The only conclusion one can come to is that not enough data exist to obtain a reasonable value of V_o. It can also be concluded, however, that the value of V_o is probably very small (less than 0.1 mm/μsec). If sufficient data did exist one could presumably use the extrapolation technique depicted in Figure 7 to obtain a reasonable value of V_o and then input this value in the equations for calculating the best value of λ.

Figure 31 shows a plot of Tmax versus V_c^R based on values from Table IX. If it is assumed that the relation between T_{max} and V_c^R can be expressed as

$$Tmax = Z\ V_c^R$$

within this pressure range, where Z is a constant, then σ_o can be approximated by the expression

$$\sigma_o = Z\ V_o$$

The data give a value of

$$Z = 35.6$$

Based on the values of V_o determined by the least-squares method, with $\lambda = 2.0$, the only probable conclusion is that

$$V_o < 0.1 \text{ mm/μsec}$$

or

$$\sigma_o < (35.6)\ (0.1) = 3.6 \text{ kb}$$

Figure 32 shows a plot of V_c^A versus V_c^R for the 5.0, 7.5, and 10.0 mil flyers. Based on the least-squares fits already discussed, it is seen that

$$V_c^A - V_c^R = 2.56\ H_p^{-1/2}$$

or

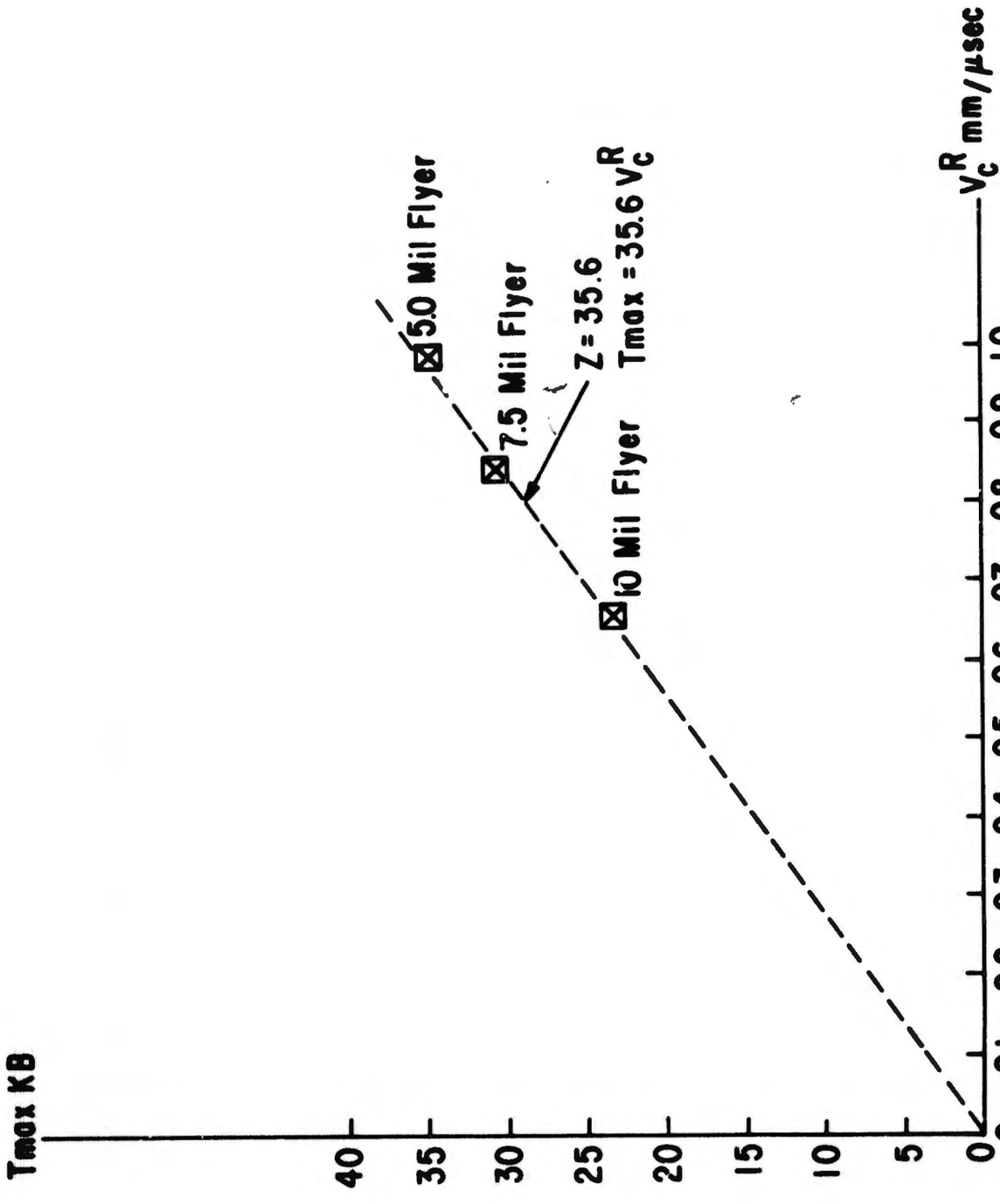

Figure 31. T_{max} versus V_c^R

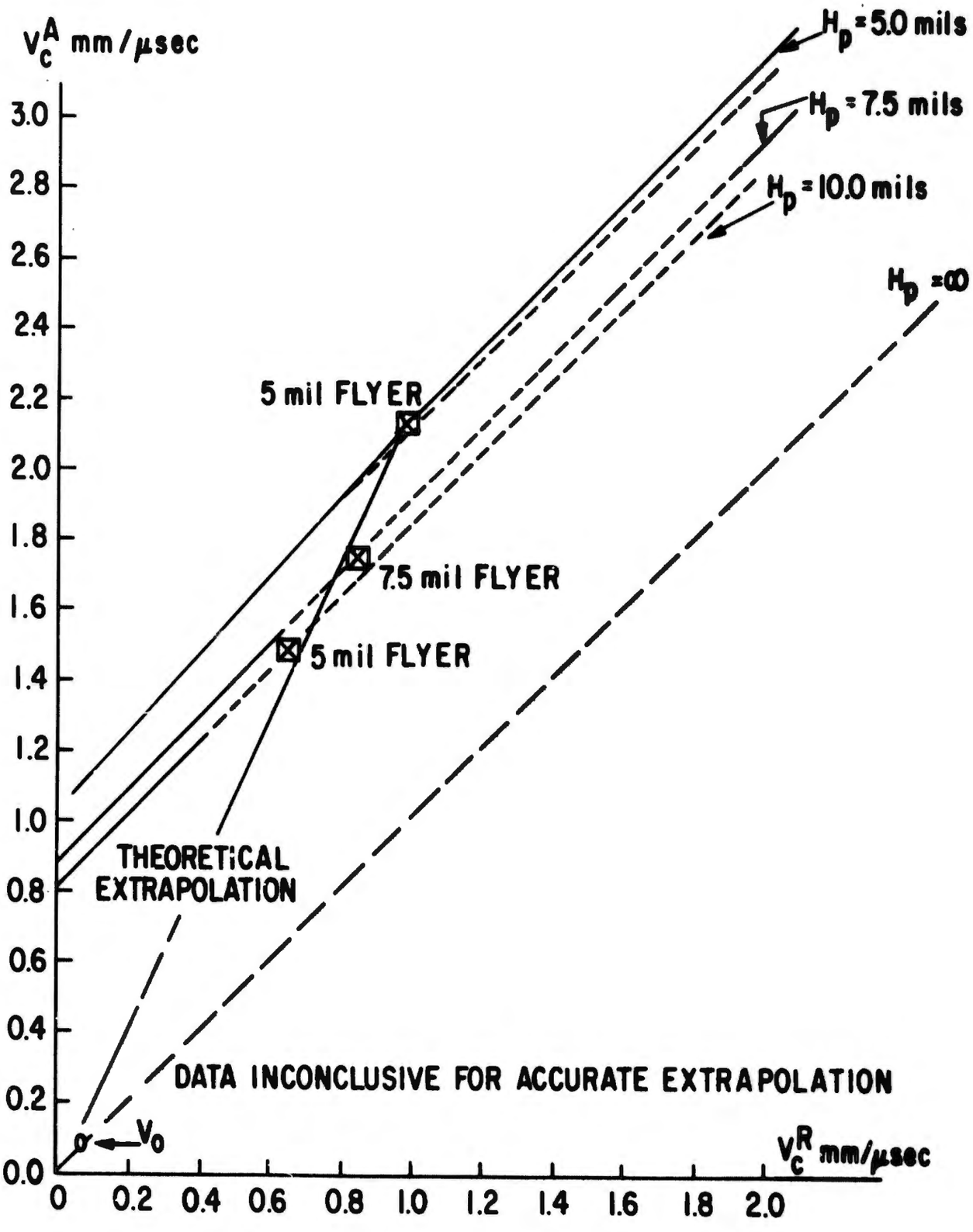

Figure 32. V_c^A versus V_c^R

$$V_c^A = V_c^R + 2.56\, H_p^{-1/2}$$

which means that for a given flyer thickness V_c^A is linearly related to V_c^R. The corresponding lines are shown plotted on Figure 32. The line with slope of unity corresponds to the limiting case of $H_p \to \infty$, where $V_c^A = V_c^R$.

It seems reasonable to assert that if more spall depth data were available, the values of $\bar{S}_2^R$ and $\bar{S}_2^A$ would approach each other as $H_p \to \infty$.

SECTION VII

CONCLUSIONS AND RECOMMENDATIONS

There is a emasurable and predictable difference between impact experiments performed in air versus vacuum environments. This difference of air layer effect reduces the amplitude, and spreads either the shock front or the entire shock duration of the stress pulse induced by the impact process. The effect appears to diminish as the flyer thickness increases (i.e., shock duration) and as the flyer velocity decreases (i.e., shock amplitude). The resultant analytic expressions for critical velocity for spall and spall depth are

$$V_c^A - V_c^R = 2.56\, H_p^{-1/2}$$

$$\bar{S}_2^A - \bar{S}_2^R = 0.30\, H_p$$

where

H_p = flyer thickness

V_c^A, V_c^R = critical velocity for spall in air and vacuum respectively,

$\bar{S}_2^A$, $\bar{S}_2^R$ = spall depth from rear surface in air and vacuum respectively.

It is possible to obtain a reasonable estimate of the dynamic material constants (λ, K) for a target material by performing impact experiments in an air environment.

For short-duration impulsive loads, the critical fracture stress was found to be a strong function of the time interval over which the tensile stress acted. Over a range of short tensile stress durations, it has been found that available data can be correlated by an equation of the form

$$\left(T_{max} - \sigma_o\right)^{\lambda} \Delta t = K$$

For 6061-T6 aluminum and for pulse widths between .06 and .12 microsecond, $\lambda = 1.8$ and $K = 34.9$. This fracture model relates to a pure energy criteria in contrast to either pure stress or impulse.

Additional work suggested by the results of this study includes (a) experiments at very short and long pulse durations and (b) collection of sufficient data to permit valid extrapolations to long pulse widths.

In addition, the following comments should be noted:

AIR LAYER EFFECT

A first source of weakness in this study may be the lack of actual shock profile measurements. If one could compare these actual profiles when an air layer was present with these conducted in vacuum, a better understanding and prediction capability would be possible. In particular, we recommend further research to determine: (a) What portion of the profile is spread out to yield essentially greater spall depths. Is the air effect influencing the shock front on the entire stress duration? (b) What is the effect of the air column thickness?

Lastly, the authors recommend some experiments to verify that region of large flyer thicknesses which is presently extrapolated to predict if there is no difference in air versus vacuum response. While all of these recommendations are vast in complexity, time consumption, and cost, AFWL is seriously considering them in an effort to enhance the state of the art of plate impact experiments.

SPALL CRITERIA

Much more rigorous and accurate verification and analysis should be made of the precise levels and mechanisms of 6061-T6 aluminum spall. Before this can be accomplished, further data are necessary. The authors recommend a continuation of this basic effort to describe failure criterion. From a theoretical standpoint, a major drawback of treating the problem of fracture for short-duration loads is the difficulty in predicting severity of cracking that can occur by the compressive pulse before passage of the damage-inducing tensile wave away from the damage area.

If extensive data for both air and vacuum environments is obtained, the techniques described in Section III for extrapolating V_c^A and V_c^R data could be accomplished to obtain values for V_o and σ_o, useful in relating (Ref. 4) at what point a material such as 6061-T6 aluminum no longer exhibits a time-dependent behavior.

APPENDIX

COMPLETE LISTING OF IMPACT DATA

This appendix enumerates the impact data, showing the flyer velocity and damage evaluation for each shot. Table XI and the resulting plots (Figures 33 and 34) show that the critical velocity for spall, V_c, was determined for each flyer thickness in both air and vacuum.

TABLE XI

TABLE OF EXPERIMENTAL DATA

(Mylar impacting 32 mil 6061-T6 aluminum; planarity -1 shots only)

Shot Number		Flyer Velocity (mm/μsec)	Result
		5 mil Mylar	
0539		2.42	spall
0558		2.12	no spall
0559		2.06	no spall
0570		2.48	spall
0571	air	2.41	spall
0575		1.91	no spall
0586		2.17	spall
0589		2.36	spall
0597		2.17	spall
0628		2.42	spall
0818		1.29	spall
0825		2.17	spall
0837		2.04	spall
0864		1.19	spall
0869		0.97	no spall
0870	vacuum	1.02	spall
0872		0.98	spall
0873		1.02	spall
0875		0.88	no spall
0876		1.11	spall
1002		1.11	spall
1005		0.76	no spall
		3 mil Mylar	
0604		3.07	spall
0611		2.64	no spall
0620	air	2.84	spall
0621		2.88	spall
0622		3.03	spall
0623		2.89	spall

TABLE XI (Cont'd)

7.5 mil Mylar

Shot Number		Flyer Velocity (mm/μsec)	Result
0544		1.84	spall
0560		1.39	no spall
0564		1.69	no spall
0576		1.88	spall
0578		1.85	spall
0588	air	1.62	no spall
0642		1.56	no spall
0646		1.68	spall
0675		1.89	spall
0676		2.02	spall
0677		2.01	spall
0827		1.72	spall
0828		1.49	spall
0842		1.37	spall
0845		0.99	spall
0848		1.25	spall
0886		1.31	spall
0889		0.75	no spall
0890		0.81	no spall
0893	vacuum	1.43	spall
0913		0.99	spall
0917		0.81	no spall
0919		0.83	no spall
0976		1.34	spall
0979		1.05	spall
0983		1.00	spall
1041		0.76	no spall
1047		0.80	no spall

TABLE XI (Cont'd)

10.0 mil Mylar

Shot Number		Flyer Velocity (mm/μsec)	Result
0524		1.42	no spall
0531		1.86	spall
0561		1.56	spall
0579		1.76	spall
0580	air	1.75	spall
0583		1.52	spall
0616		1.48	no spall
0617		1.46	no spall
0618		1.33	no spall
0619		1.59	spall
0840		1.50	spall
0897		1.12	spall
0898		0.91	spall
0900		0.73	spall
0901		0.65	spall
0902	vacuum	0.66	spall
0927		0.63	no spall
0929		0.65	spall
0934		0.53	no spall
0937		0.55	no spall
0940		0.55	no spall
0941		0.65	no spall

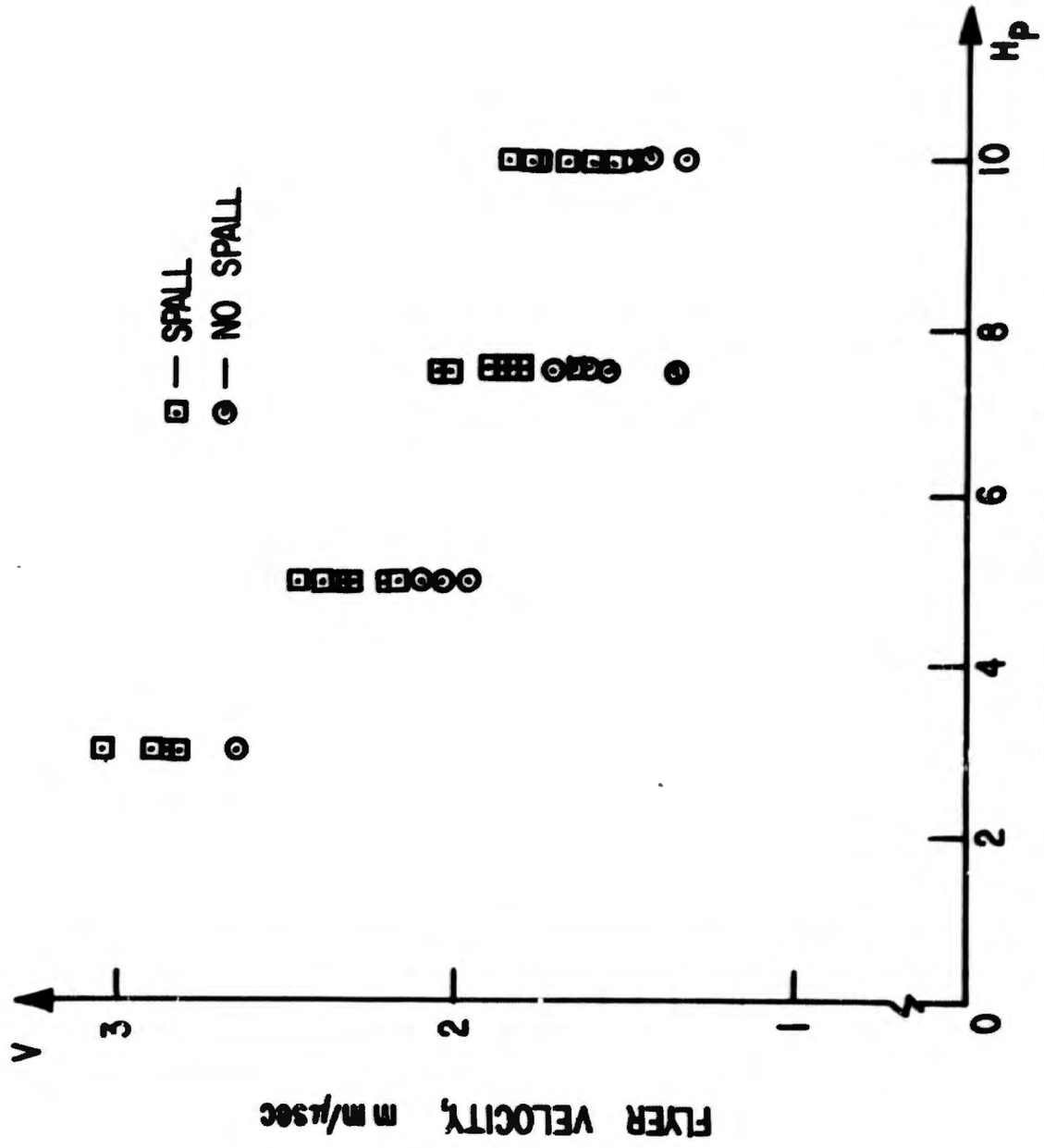

Figure 33. Experimental Data from Air Environment

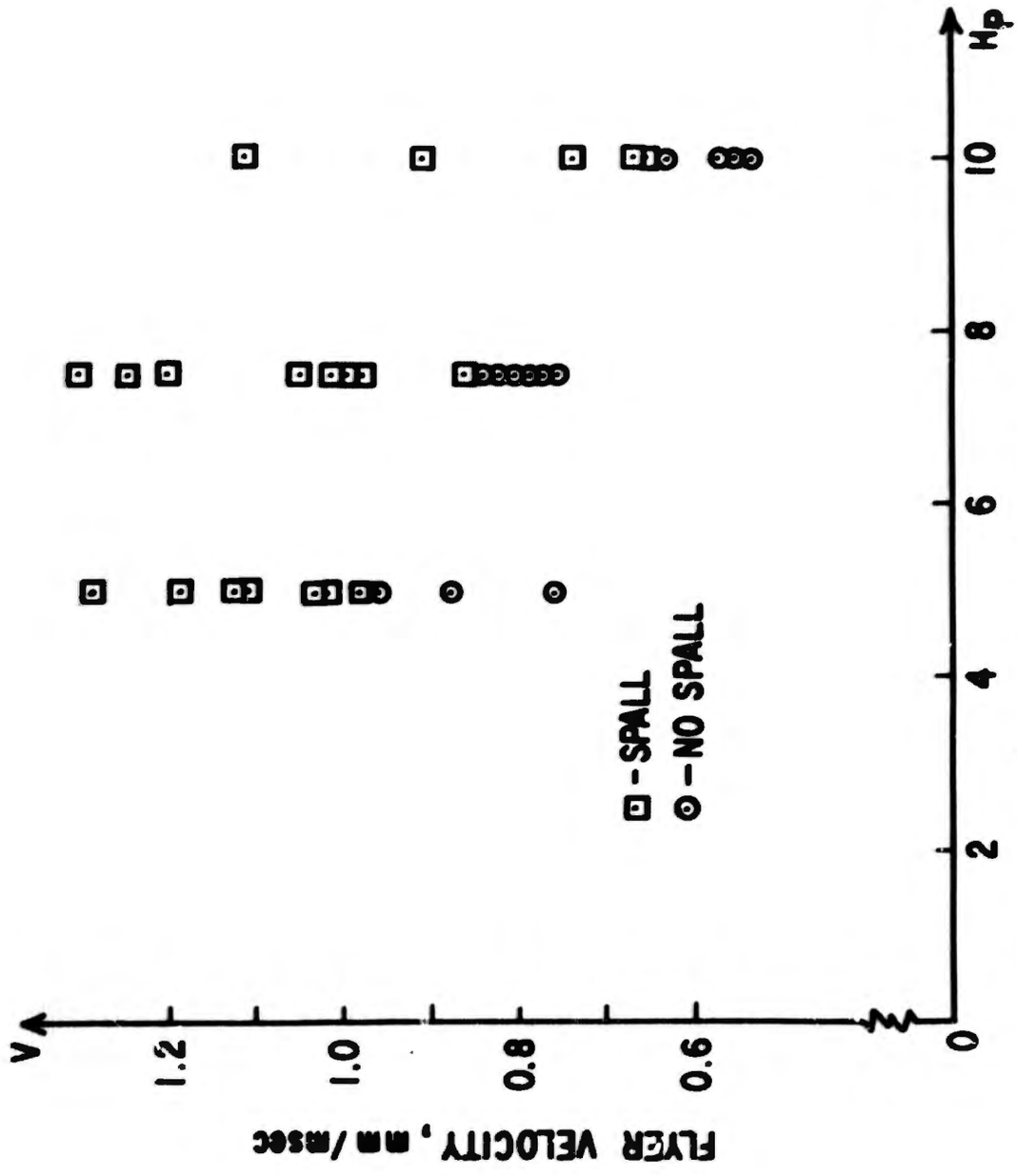

Figure 34. Experimental Data from Vacuum Environment

REFERENCES

1. Baca, Jose R., Determination of Spallation Thresholds by Exploding Foil Techniques, Thesis, Air Force Institute of Technology, June 1968.

2. Butcher, B. M., Spallation in 6061-T6 Aluminum, Preprint SC-DC-66-2448, Sandia Laboratory, New Mexico.

3. Brodie, R. N., Hormuth, J. E., The PUFF and P-PUFF 66 Computer Programs, AFWL-TR-66-48, Air Force Weapons Laboratory, Kirtland AFB, NM, May 1966.

4. Lundergan, C. D., The Equation of State of 6061-T6 Aluminum at Low Pressures, Research Report SC-4637, Sandia Corporation, New Mexico, September 1961.

5. Butcher, B. BM., Tuler, F. R., "A Criterion for the Time Dependence of Dynamic Fracture," Internat. J. Frac. Mech., Vol. IV, No. 4, p. 431, December 1968.

6. Breed, R. B., Mader, C. L., Venable, D., "Technique for the Determination of Dynamic-Tensile-Strength Characteristics," J. Appl. Phys., 38, p. 3271, 1967.

7. Berkowitz, H. M., Cohen, L. J., Peck, J. C., The Relationship of the Critical Stress versus Impulse Theory of Spall Fracture to Stress-Gradient or Stress-Rate Theories, McDonnell Douglas Astronautics Company, Santa Monica, California

8. Wunsch, D. C., et al., Acceleration of Thin Plates by Exploding Foil Techniques, AFSWC-TDR-61-75, Air Force Special Weapons Center, Kirtland AFB, NM, January 1961.

9. Weis, C., Analysis of Flyer Plate Experiments, AFSWC-TDR-61-74, Air Force Special Weapons Center, Kirtland AFB, NM, January 1961.

This page intentionally left blank.

UNCLASSIFIED

Security Classification

DOCUMENT CONTROL DATA - R & D

(Security classification of title, body of abstract and indexing annotation must be entered when the overall report is classified)

1. ORIGINATING ACTIVITY (Corporate author) Air Force Weapons Laboratory (WLRP) Kirtland Air Force Base, New Mexico 87117	2a. REPORT SECURITY CLASSIFICATION UNCLASSIFIED 2b. GROUP

3. REPORT TITLE

SPALL STUDIES ON 6061-T6 ALUMINUM

4. DESCRIPTIVE NOTES (Type of report and inclusive dates)

January 1968 to March 1969

5. AUTHOR(S) (First name, middle initial, last name)

Charles Jajosky, Jr., Capt, USAF; Mark A. Ferdman, Lt, USAF

6. REPORT DATE September 1969	7a. TOTAL NO. OF PAGES 90	7b. NO. OF REFS 9
8a. CONTRACT OR GRANT NO. b. PROJECT NO. 5710 c. Subtask 15.025 d.	9a. ORIGINATOR'S REPORT NUMBER(S) AFWL-TR-69-101 9b. OTHER REPORT NO(S) (Any other numbers that may be assigned this report)	

10. DISTRIBUTION STATEMENT This document is subject to special export controls and each transmittal to foreign governments or foreign nationals may be made only with prior approval of AFWL (WLRP), Kirtland AFB, NM. Distribution is limited because of the technology discussed in the report.

11. SUPPLEMENTARY NOTES	12. SPONSORING MILITARY ACTIVITY AFWL (WLRP) Kirtland AFB, NM 87117

13. ABSTRACT (Distribution Limitation Statement No. 2)

Flat specimens of 32 mil 6061-T6 aluminum were dynamically shock loaded by high velocity Mylar flyer plates. A 16 kilojoule capacitor discharge system and exploding foil assemblies were used to accelerate 3, 5, 7.5, and 10 mil Mylar flyers at spall threshold velocities between 0.5 and 2 mm/μsec. The environment between flyer and target was both normal and atmospheric air and vacuum. The observed apparent spall threshold and spall depths in air differed significantly from those obtained in vacuum. The air layer has the effect of reducing the amplitude of the induced stress pulse and spreading the shock front and/or its pulse duration. The spall threshold data were analyzed and an attempt was made to apply available predictive models. The data best fit the Tuler, et al., model, with a stress exponent of 1.8. This condition very closely approximates a pure-energy criterion for spallation.

DD FORM 1 NOV 68 1473

UNCLASSIFIED

Security Classification

14. KEY WORDS	LINK A		LINK B		LINK C	
	ROLE	WT	ROLE	WT	ROLE	WT
Spall Hugoniot Flyer plate 6061-T6 aluminum Failure criterion P-PUFF						